Reports of the Department of Geodetic Science and Surveying
Report No. 368

LEAST SQUARES COLLOCATION APPLIED TO LOCAL GRAVIMETRIC SOLUTIONS FROM SATELLITE GRAVITY GRADIOMETRY DATA

by
John W. Robbins

Prepared for
National Aeronautics and Space Administration
Goddard Space Flight Center
Greenbelt, Maryland 20770

NASA Grant No. NGR 36-008-161
OSURF Project 783210

The Ohio State University
Department of Geodetic Science and Surveying
1958 Neil Avenue
Columbus, Ohio 43210

August, 1985

ABSTRACT

An autonomous spaceborne gravity gradiometer mission is being considered as a post Geopotential Research Mission project. The introduction of satellite gradiometry data to geodesy is expected to improve our solid earth gravity models. This study explores the possibility of utilizing gradiometer data for the determination of pertinent gravimetric quantities on a local basis. The analytical technique of least squares collocation is investigated for its usefulness in local solutions of this type. It is assumed, in the error analysis, that the vertical gravity gradient component of the gradient tensor is used as the raw data signal from which the corresponding reference gradients are removed to create the centered observations required in the collocation solution. The reference gradients are computed from a high degree and order geopotential model. The solution can be made in terms of mean or point gravity anomalies, height anomalies, or other useful gravimetric quantities depending on the choice of covariance types. Selected for this study were 30′x30′ mean gravity and height anomalies. Existing software and new software are utilized to implement the collocation technique. It was determined that satellite gradiometry data at an altitude of 200 km can be used sucessfully for the determination of 30′x30′ mean gravity anomalies to an accuracy of 9.2 mgal from this algorithm. It is shown that the resulting accuracy estimates are sensitive to gravity model coefficient uncertainties, data reduction assumptions and satellite mission parameters.

FOREWORD

This report was prepared by John W. Robbins, Graduate Research Associate, Department of Geodetic Science and Surveying, The Ohio State University under NASA Grant NGR36-008-161, The Ohio State University Research Foundation Project No. 783210. This project is under the direction of Professor Richard H. Rapp. The grant covering this research is administered through the NASA Goddard Space Flight Center, Greenbelt, Maryland 20771. The NASA Technical Officer for this grant is Mr. Jean Welker, Code 621.

This report is also being submitted to the Graduate School of The Ohio State University in partial fulfillment of the requirements for the degree of Master of Science.

The reproduction and distribution of this report was carried out with funds supplied, in part, by the Department of Geodetic Science and Surveying.

ACKNOWLEDGEMENTS

First, I would like to thank Professor Richard Rapp for his advice and support throughout the project. His carefully considered comments and suggestions considerably strengthened this work.

I also wish to thank my colleagues for showing interest and listening to my ideas. Particularly, Theo Engelis and Steve Hilla received the brunt of my thoughts. Our discussions always lead to further insight on all levels of this work.

My gratitude goes to Christian Tscherning for sharing his philosophy and providing suggestions. I am most grateful for his assistance with his program COVAX. A word of thanks must also go to Dr. Roger Hastings of the Sperry Corporation and Dr. Victor Reinhardt of Hughes Aerospace for providing copies of their reports concerning the development of their respective gradiometers.

The computing center of Ohio State University, IRCC, provided the computing services to support this study.

Many thanks go to Tracy Runyon for her expedient and dependable typing of this report.

Finally, my deepest gratitude is extended to my mother and late father who have instilled within me an unending sense of curiosity and who have encouraged me to attain educational fulfillment.

TABLE OF CONTENTS

APPENDICES

LIST OF TABLES

LIST OF FIGURES

I. INTRODUCTION

Gravimetric geodesy is in the midst of a period of rapid growth. During the last twenty-five years, geodetic information has grown formidably, primarily due to the application of space technology. With proper guidance and funding, this trend will continue at a pace unimaginable to those scientists involved at the beginning of the space age. Currently, many countries have offerred support for the rapid growth of geodetic science. In the United States, geodetic progress is made by many government agencies, universities and private corporations who are involved in a wide variety of projects. Perhaps the largest civilian endeavor is one under the auspices of the National Aeronautics and Space Administration known as the The Geodynamics Project. The objectives of this project, as outlined in NASA [1983], are:

"(1) to contribute to the understanding of the solid Earth, in particular the processes that result in movement and deformation of tectonic plates; and

(2) to improve measurements of the Earth's rotational dynamics and its gravity and magnetic fields".

These two objectives are inextricably related and perhaps a third objective could be included;

(3) to form a useful geophysical information data base for the use of studies in advanced Earth geophysics as well as absolute and comparative planetology.

Thus the primary objectives could be reformed into the single sentence: The primary goal of The Geodynamics Project is to formulate solid-Earth

models which more accurately depict the geophysical nature of our planet.

Several types of observable phenomena exist which contribute to the formulation of solid-Earth models. Two such phenomena are the geopotential fields, the gravity and magnetic fields of the Earth. In this study, the gravity field is highlighted as the phenomenon of basic interest. An interesting number of by-products, or applications, can be made from the study of the Earth's gravitational potential (or, for short, the geopotential). These applications are nicely summarized in the NRC publication, Applications of a Dedicated Gravitational Satellite Mission (National Academy of Science [1979]).

The rationale for improving and increasing the knowledge of the Earth's geopotential comes from many sources. Some examples include:

Geophysics: Gravity information is used to infer isostatic information to supplement and constrain tectonic models. Geoid undulations can be correlated with density anomalies to constrain mantle convection models.

Oceanography: Highly accurate geoid models when used with altimetric data yield precise knowledge on the sea surface topography which is useful in the determination of local ocean circulation patterns. With altimeter measurements over a period of time, a fourth or dynamic dimension can be included which may improve the understanding of the meteorological/ocean circulation interface.

As can be seen from these few examples, improvements in gravity field knowledge have strong repurcussions within the geophysical community which can ultimately contribute to a unified earth model. There are certain geodetic applications which would benefit from improved gravitational potential knowledge. The major impetus stems from the

need to improve the accuracy of artificial satellite ephemerides. Many NASA projects being considered rely heavily upon how accurately a satellite orbit can be determined. Altimetry projects (such as TOPEX), mapping projects (such as MAPSAT), and other remote sensing missions are some examples of missions requiring precise orbits.

With this brief introduction, some examples supporting the rationale for gravity model improvements have been mentioned. It is then worthwhile to describe a few of the projects currently under consideration to directly improve our gravity field knowledge.

NASA is currently considering two types of instruments to be used in a gravity field measurment campaign; Satellite-to-Satellite tracking (SST) techniques are to be used in the Geopotential Research Mission (GRM); and satellite gravity gradiometry utilizing cryogenic technology is to be used in a follow on mission. The Satellite-to-Satellite tracking instrumentation is described in APL [1983] and a proposal for recovering geopotential information is discussed in Colombo [1984]. Satellite borne gravity gradiometers (the instrument of primary interest in this work) are summarized in Wells [1984]. Instrument descriptions and gradiometry theory will be discussed in the next chapter.

It should be stressed that the two types of instrumentation (SST and gradiometry) are not competitive with one another. Rather, they are complementary since they are individually sensitive to different wavelengths of the gravity field. This is evident in Figures 1a and 1b which were generated by the rapid error analysis procedure described in Jekeli and Rapp [1980]. The graph illustrates mean gravity anomaly accuracy estimates from the six month GRM mission as well as those from a six month gradiometry missions. It can be seen in Figure 1a that higher resolution is achieved when the sensitivity of the instrument is increased. Higher resolution is also achieved when the satellite altitude is lowered (Fig. 1b) such as proposed in the space shuttle tether system (NASA [1984]) which would allow for altitudes near 140 kilometers. Thus

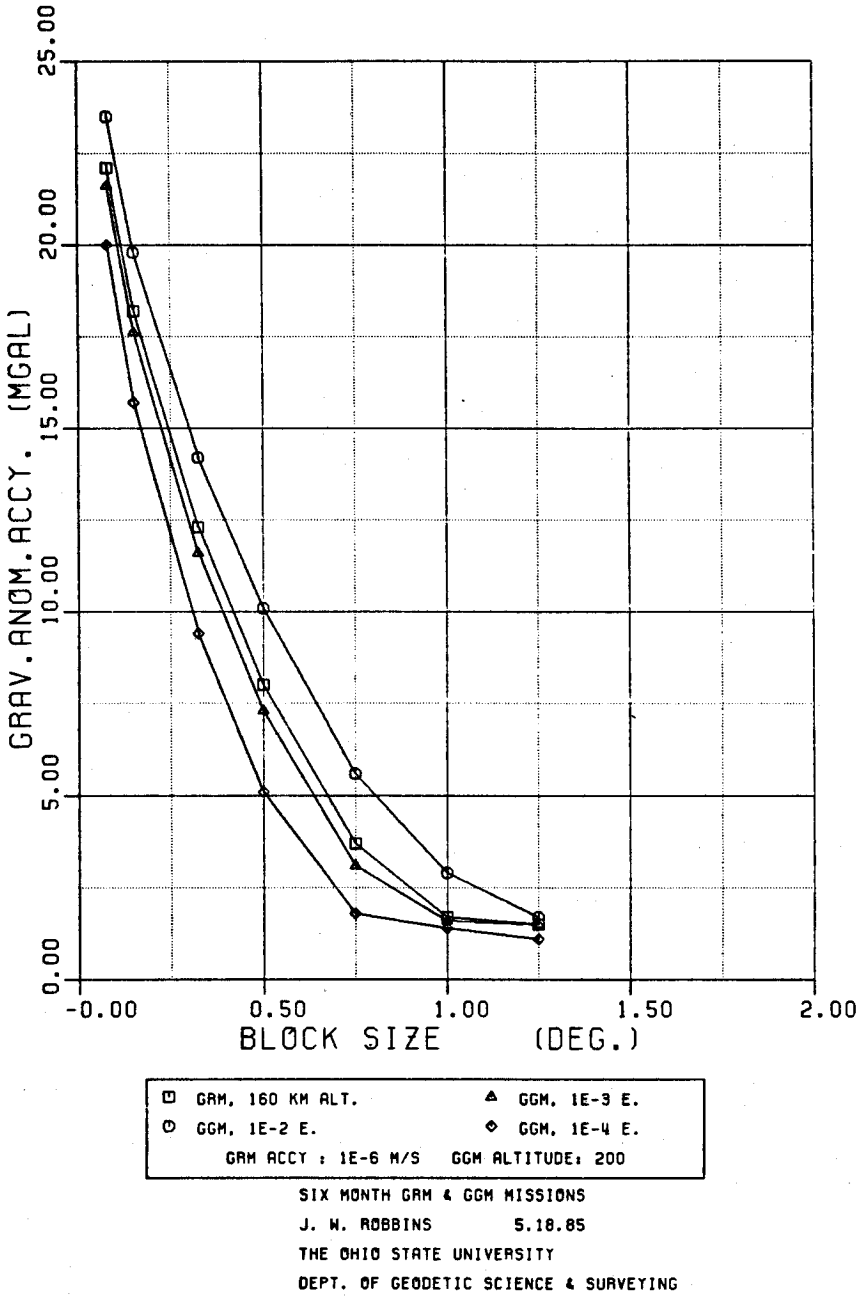

Figure 1a. Expected mean gravity anomaly accuracies from GRM and gradiometry plotted by instrument sensitivity (200 km altitude assumed for the gradiometer).

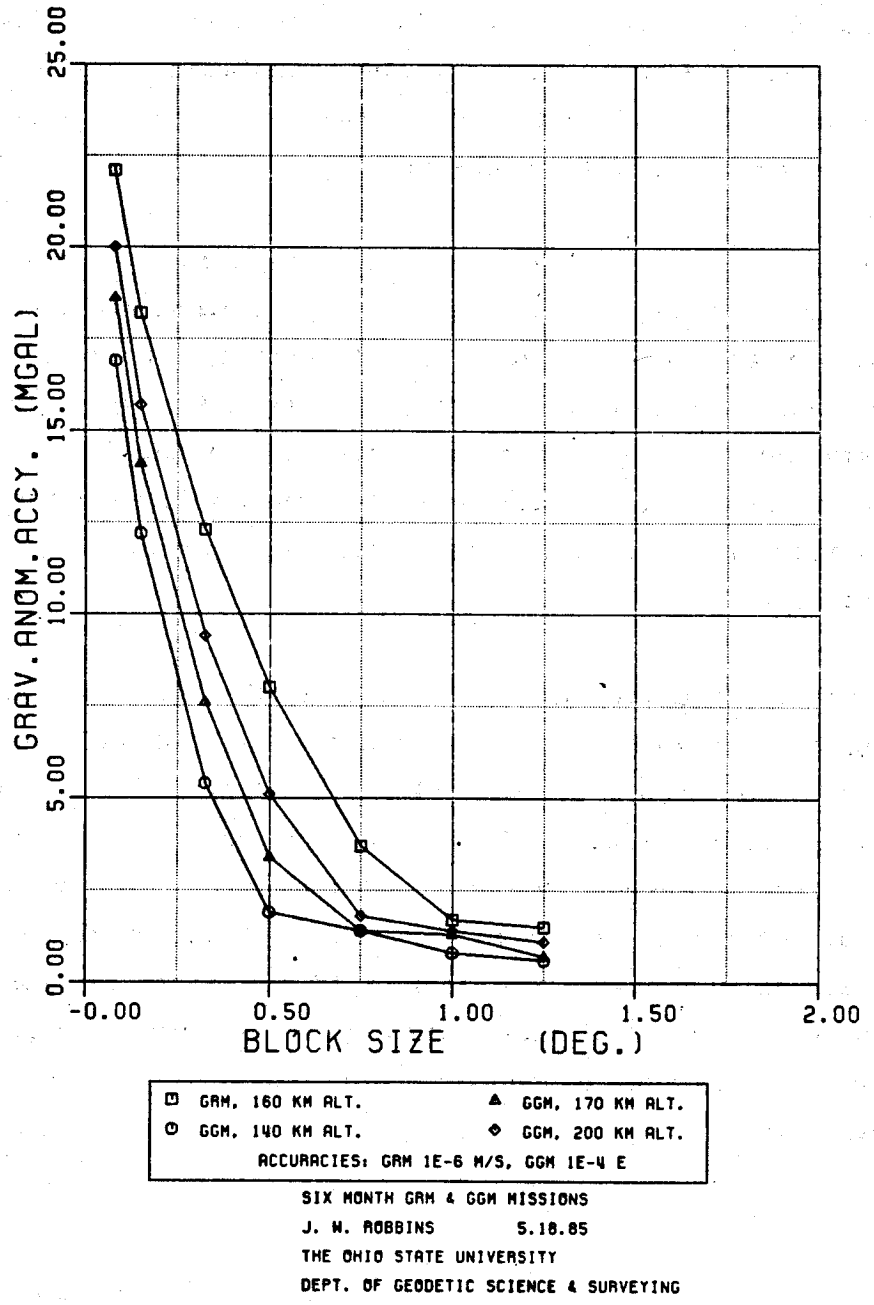

Figure 1b. Expected mean gravity anomaly accuracies from gradiometry plotted by altitudes of 140, 170, and 200 km.

if the GRM project is fully supported, then the follow-on gravity gradiometry mission, if it is also supported, will be under strict instrumentation and altitude requirements in order to make significant improvements in spatial resolution.

In this work, the prospect of utilizing local (as opposed to global) gradiometry data for the estimation of mean gravity anomalies and height anomalies is explored. The theoretical foundation is supplied by least-squares collocation theory. The idea of using only local information was advanced due to the substantial computer effort required in global solutions. The purpose of this work is to test a local collocation algorithm for its accuracy, dependability, and ease of operation.

The next chapter introduces the satellite gravity gradiometer (SGG) concept along with the units and coordinate systems involved. Mentioned too, are the design concepts, likely mission profiles, and a review of previous reduction methods. In chapter three, the general theory of collocation as applied to the local gradiometry reduction is expounded. The use of a high degree and order geopotential model will be explained. Chapter four presents the results of the error analysis and ensuing discussion. The final chapter attempts to provide a perspective of this work by drawing conclusions and suggesting alternative lines of investigation.

2. REVIEW OF GRADIOMETRY, ITS INSTRUMENTS AND METHODS

2.1 Concepts and Theory

The basic theory behind gradiometers has been known since the early days of torsion balances, when around 1900 a Hungarian physicist, Roland Eötvös, developed a working variometer. Torsion balances had wide spread use during the 1920's for geophysical exploration. Their use declined due to the introduction of the more economical gravimeter. However, torsion balance measurements are still being made today but they are rapidly becoming obsolete with the influx of high technology gradiometers and inertial systems.

In order to intuitively appreciate the concepts underlying gradiometry, it may be worthwhile to discuss the theory, units and physical interpretation behind this system. A gravity gradiometer is capable of sensing and recording the values of the spatial second derivatives of the gravitational potential. The discussion begins by recalling that the potential is a scalar quantity having SI-units of m^2s^{-2}. The first spatial derivative of the potential is generally associated with gravitation which is an acceleration quantity or vector quantity having units of ms^{-2}. Acceleration can be intuitively described as the rate of change of an object's velocity. The second spatial derivative of the potential is also a vector quantity which has units of s^{-2}. These units may seem physically meaningless at first, but it is easy to recognize that the second spatial derivative allows for a description of the spatial variation of the gravitational acceleration. For instance, the unit most often associated with these second derivatives is the Eötvös (denoted E). One Eötvös is 10^{-9} s^{-2} which can be thought of as 10^{-9} ms^{-2}/m. In words, this means that one Eötvös is a change of

10^{-9} ms^{-2} over a one meter distance. In more familiar gravity units, one Eötvös is equivalent to a 0.1 mgal change over one kilometer.

The nine spatial second derivatives of the gravitational potential constitute the "gravity gradient tensor" which is conveniently expressed in matrix form by

$$\begin{bmatrix} V_{11} & V_{12} & V_{13} \\ V_{21} & V_{22} & V_{23} \\ V_{31} & V_{32} & V_{33} \end{bmatrix} \tag{II.1}$$

where V denotes the gravitational potential of a body and the subscripts refer to the spatial derivatives (eg. $V_{11} = \partial^2 V/\partial x_1^2$, $V_{12} = \partial^2 V/\partial x_1 \partial x_2$, etc.). The 1, 2, 3-subscripts refer to directions associated with an orthogonal coordinate system. As long as the directions remain orthogonal, then the gravity gradients along these directions must satisfy Laplace's equation,

$$\sum_{i=1}^{3} V_{ii} = 0 \tag{II.2}$$

that is, the diagonal elements of the gravity gradient tensor are subject to Laplace's condition.

The formulation of the potential by spherical harmonics begins by defining a geocentric coordinate system. Let the X_3-axis of a geocentric Cartesian coordinate system coincide with the mean rotation axis of the earth. Next, let the X_1-axis lie in the mean equatorial plane as well as in the plane formed by the Greenwich meridian. The X_2-axis completes the right handed Earth fixed Cartesian system by lying in the mean equatorial plane in the direction of longitude $\pi/2$. The geocentric spherical coordinates (ϕ, λ, r) follow immediately which are defined as shown in Figure 2. The earth's gravitational potential can then be written in spherical harmonic form as

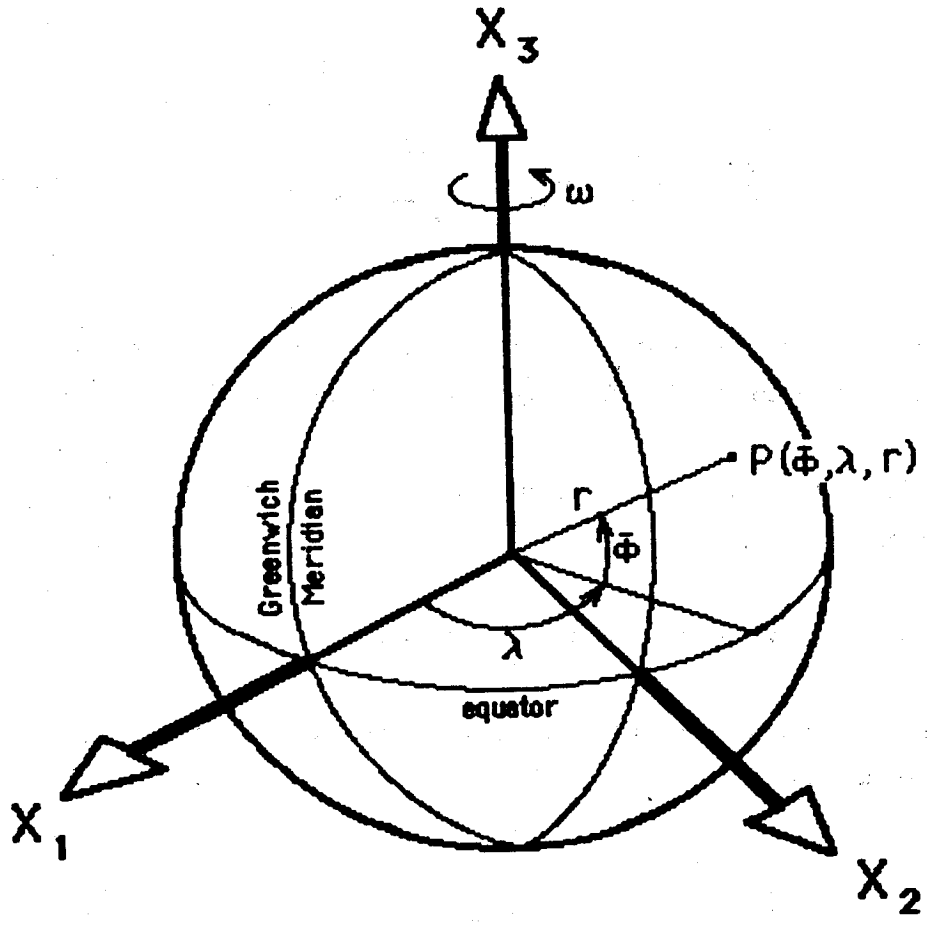

Figure 2. Geocentric cartesian and spherical coordinate systems

$$V(\bar{\phi},\ \lambda,\ r) = \frac{GM}{r}\left[1 + \sum_{n=2}^{\infty}\left(\frac{a}{r}\right)^n \sum_{m=0}^{n}(\bar{C}_{nm}\cos m\lambda + \bar{S}_{nm}\sin m\lambda)\bar{P}_{nm}(\sin\bar{\phi})\right] \qquad (II.3)$$

where $\bar{C}_{nm}$, $\bar{S}_{nm}$ are the normalized potential coefficients, $\bar{P}_{nm}(\sin\bar{\phi})$ are the normalized associated Legendre functions, a is a mean equatorial radius value for the earth (e.g. 6378137 m for the 1980 Geodetic Reference System) and r is the radial distance of the computation point at latitude $\bar{\phi}$ and longitude λ. Similarly, an expression for the reference gravitational potential can be written as

$$U(\bar{\phi}, \lambda, r) = \frac{GM}{r}\left[1 + \sum_{n=2}^{N}\left(\frac{a}{r}\right)^n \sum_{m=0}^{n}(\bar{C}'_{nm}\cos m\lambda + \bar{S}'_{nm}\sin m\lambda)\bar{P}_{nm}(\sin\bar{\phi})\right] \tag{II.4}$$

where the primes denote reference potential coefficients which are approximations to the $\bar{C}_{nm}$, $\bar{S}_{nm}$ in equation (II.3).

The disturbing potential, in the present notation is, in the well known formula,

$$T(\bar{\phi}, \lambda, r) = V(\bar{\phi}, \lambda, r) - U(\bar{\phi}, \lambda, r) \tag{II.5}$$

The disturbing potential can also be written in a spherical harmonic expansion as:

$$T(\bar{\phi}, \lambda, r) = \frac{GM}{r}\left[\sum_{n=2}^{N}\left(\frac{a}{r}\right)^n \sum_{m=0}^{n}(\varepsilon\bar{C}_{nm}\cos m\lambda + \varepsilon\bar{S}_{nm}\sin m\lambda)\bar{P}_{nm}(\sin\bar{\phi}) + \sum_{n=2}^{\infty}\left(\frac{a}{r}\right)^n \sum_{m=0}^{n}(\bar{C}_{nm}\cos m\lambda + \bar{S}_{nm}\sin m\lambda)\bar{P}_{nm}(\sin\bar{\phi})\right] \tag{II.6}$$

where here the $\varepsilon\bar{C}_{nm}$ and $\varepsilon\bar{S}_{nm}$ terms are the discrepancies between the coefficients of the true field and the coefficients of the reference field. That is, more explicitly,

$$\begin{aligned}\varepsilon\bar{C}_{nm} &= \bar{C}_{nm} - \bar{C}'_{nm} \\ \varepsilon\bar{S}_{nm} &= \bar{S}_{nm} - \bar{S}'_{nm}\end{aligned} \tag{II.7}$$

These discrepancies are better termed "coefficient errors" which implies that the reference (or "model") coefficients are in error with respect to the unknown "true" coefficients (Colombo, [1980]). Since the coefficient errors cannot be found directly, they are approximated by the a posteriori variances for the computed model coefficients. These errors will play a significant role in the covariance computations discussed in Section III.4.

Next, the spatial derivatives of the various potential expressions will be examined. A connection between the well known principles of gravimetric geodesy and the spatial derivatives will be highlighted to provide an intuitive framework.

The first spatial derivatives of (II.3) can be related to the components of gravity by (Heiskanen and Moritz [1967])

$$g_{X_1} = V_{X_1} + \Phi_{X_1}, \quad g_{X_2} = V_{X_2} + \Phi_{X_2}, \quad g_{X_3} = V_{X_3} + \Phi_{X_3} \tag{II.8}$$

where Φ denotes the centrifugal potential. Similarly, the components of the reference (or normal) gravity are;

$$\gamma_{X_1} = U_{X_1} + \Phi_{X_1}, \quad \gamma_{X_2} = U_{X_2} + \Phi_{X_2}, \quad \gamma_{X_3} = U_{X_3} + \Phi_{X_3}. \tag{II.9}$$

The gravity disturbance, $\vec{\delta}$ is defined as the difference between the true (measured) gravity, $\vec{g}$ and the reference (modeled) gravity $\vec{\gamma}$, (Heiskanen and Moritz [1967], section 6-1)

$$\vec{\delta} = \vec{g} - \vec{\gamma} \tag{II.10}$$

Then, in geocentric Cartesian coordinates, the gravity disturbance components are (since the centifugal potential terms cancel):

$$\begin{aligned}
\delta_{X1} &= \frac{\partial V}{\partial X_1} - \frac{\partial U}{\partial X_1} = g_{X1} - \gamma_{X1} = \frac{\partial T}{\partial X_1} \\
\delta_{X2} &= \frac{\partial V}{\partial X_2} - \frac{\partial U}{\partial X_2} = g_{X2} - \gamma_{X2} = \frac{\partial T}{\partial X_2} \\
\delta_{X3} &= \frac{\partial V}{\partial X_3} - \frac{\partial U}{\partial X_3} = g_{X3} - \gamma_{X3} = \frac{\partial T}{\partial X_3}
\end{aligned} \qquad \text{(II.11)}$$

It is possible to differentiate each equation in (II.11) with respect to the three directions thus yielding the nine anomalous tensor components referred to the geocentric cartesian system

$$\begin{bmatrix}
T'_{11} = \frac{\partial}{\partial X_1}(\delta_{X_1}) & T'_{12} = \frac{\partial}{\partial X_2}(\delta_{X_1}) & T'_{13} = \frac{\partial}{\partial X_3}(\delta_{X_1}) \\
T'_{21} = \frac{\partial}{\partial X_1}(\delta_{X_2}) & T'_{22} = \frac{\partial}{\partial X_2}(\delta_{X_2}) & T'_{23} = \frac{\partial}{\partial X_3}(\delta_{X_2}) \\
T'_{31} = \frac{\partial}{\partial X_1}(\delta_{X_3}) & T'_{32} = \frac{\partial}{\partial X_2}(\delta_{X_3}) & T'_{33} = \frac{\partial}{\partial X_3}(\delta_{X_3})
\end{bmatrix} \qquad \text{(II.12)}$$

where the primes denote that the gradients are referred to the geocentric coordinate system. This equation illustrates how the gravity disturbances are related to the anomalous gravity gradients referred to the geocentric cartesian system. The anomalous gravity gradients are then the spatial rates of change of the gravity disturbances.

It is expected that the gravity gradient observation will be referred to a local level cartesian coordinate system. In this coordinate system, the x_3-axis coincides with the radius vector in the spherical case (Fig. 3). The x_2-axis is oriented in a northerly direction and the x_1-axis in

an easterly direction such that

$$\frac{\vec{x}_1}{|x_1|} \times \frac{\vec{x}_2}{|x_2|} = \frac{\vec{x}_3}{|x_3|} \qquad \text{(II.13)}$$

The curvature parameters of the level surfaces and the plumb line can be developed with regards to this local level system (Heiskanen and Moritz [1967], section 2.2).

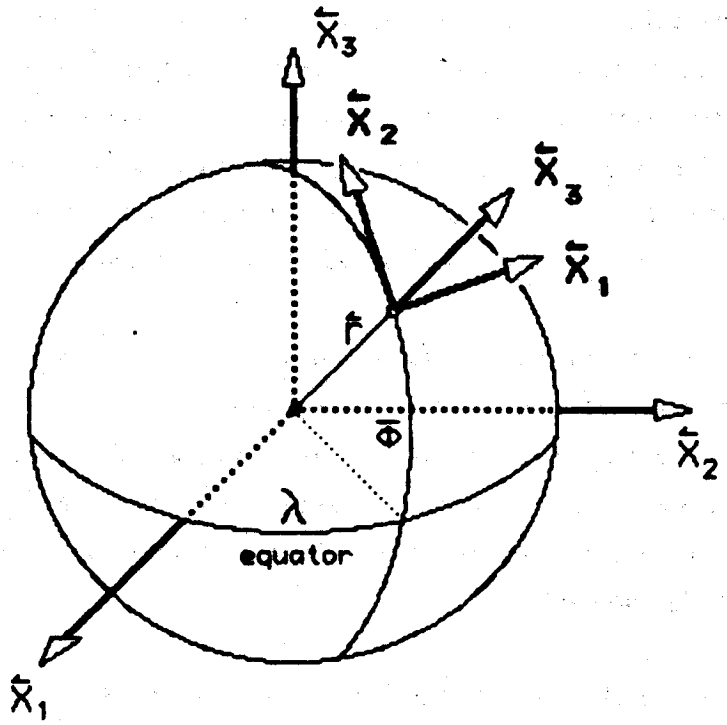

Figure 3. Local level cartesian coordinate system, x_i

2.2 Instrumentation

For the sake of comprehensiveness, a brief overview of satellite gravity gradiometer instrumentation is provided in this work. The discussion is by no means complete but only serves to increase the reader's awareness of the measurment principles involved and the accuracies obtainable by the proposed instruments. References will be made throughout to aid the reader's desire for details.

At present, two very good reviews of instrument theory and design exist. The first one by Forward [1974], presents a good historical perspective of gradiometer mission and system development up to the date of publication. Several types of designs are presented ranging from quartz balance systems, vibrating string systems, to rotating resonant torsional gradiometers. Since the review by Forward, applications of new technologies have shown remarkable improvements in gradiometry design. These new generation gradiometer systems are reviewed in Wells [1984]. This section attempts to highlight some of the designs mentioned in this more recent publication.

In the United States, there are a number of research groups investigating gradiometer instrumentation (Table 1). Some of the groups have experienced continuous funding from various agencies for the purpose of development, others have had their funding cut-off. Thus this overview will contain only those groups known by the author to be actively funded.

Basically there are two types of gradiometry sensors; Conventional and Cryogenic. Conventional sensors operate at room temperature and may have a higher level of maturity than cryogenic sensors which operate at very low temperatures (less than 4.2° Kelvin, the boiling point of liquid Helium at one atmosphere). Only two of the organizations listed in Table 1 are developing conventional gradiometers, these are Bell Aerospace and Hughes.

The Bell Aerospace gradiometer utilizes a slowly rotating platform on which are mounted four accelerometers (Fig. 4). The gravity gradients are measured by differencing the outputs of opposing accelerometers. Due to the rotation of the platform, the gradient signal is sinusoidally modulated with a period at twice the rotational period. The use of four accelerometers facilitates the detection of minute gravity gradients by utilizing "common mode rejection of the large acceleration" (Metzger & Jincitano, [1981]). An orbital mission system has been proposed by Bell which utilizes the same instrument concept. Miniature electrostatic accelerometers (MESA's) are to replace the current operational accelerometers (the Mark VII). It has been reported that the MESA based gradiometer will have much lower noise levels than the current operational system (the MESA based system has an estimated noise level of around 0.035E (Wells [1984], p. 32)).

The Hughes gradiometer is also a rotating instrument but the system design is quite different from the Bell gradiometer. The observable quantity is the strain due to the torsional flexure experienced by the resonant cruciform mass-spring system (Fig. 5). The torsional flexure is coupled to the differential torque experienced between the two arms. Since the system is rotating, the differential torques, due to the gradients of the gravitational field, are excited at a frequency twice that of the system rotation frequency. The differential torque, ΔT, is related to the gravity gradients through the following expression

$$\Delta T = \frac{m\ell^2}{4} [(V_{xx} - V_{yy})\cos 2\omega t + 2V_{xy}\sin 2\omega t] \qquad (II.14)$$

where all terms are defined as illustrated in Figure 5 and where the x and y directions lie in the plane of rotation. The system noise level goal is 0.01E (1σ) using a 35 second integration time. It was not

Table 1

Organizations Active in Gravity Gradiometer R & D.

Organization	Gradiometer Type	Principle Investigators
Bell Aerospace	Rotating Accelerometer	Metzger/Jincitano
Bendix/Stanford Univ.	Superconducting Cavity Oscillators	Reinhardt/ Turneaure
Hughes	Rotating Gravity Gradiometer	Forward
SAO/PSN	Gravity Radiation	
Sperry Defense Syst.	Cryogenic Levitated Balance Arm	Hastings
Univ. of Maryland	Superconducting Accelerations with SQUID readout	Paik

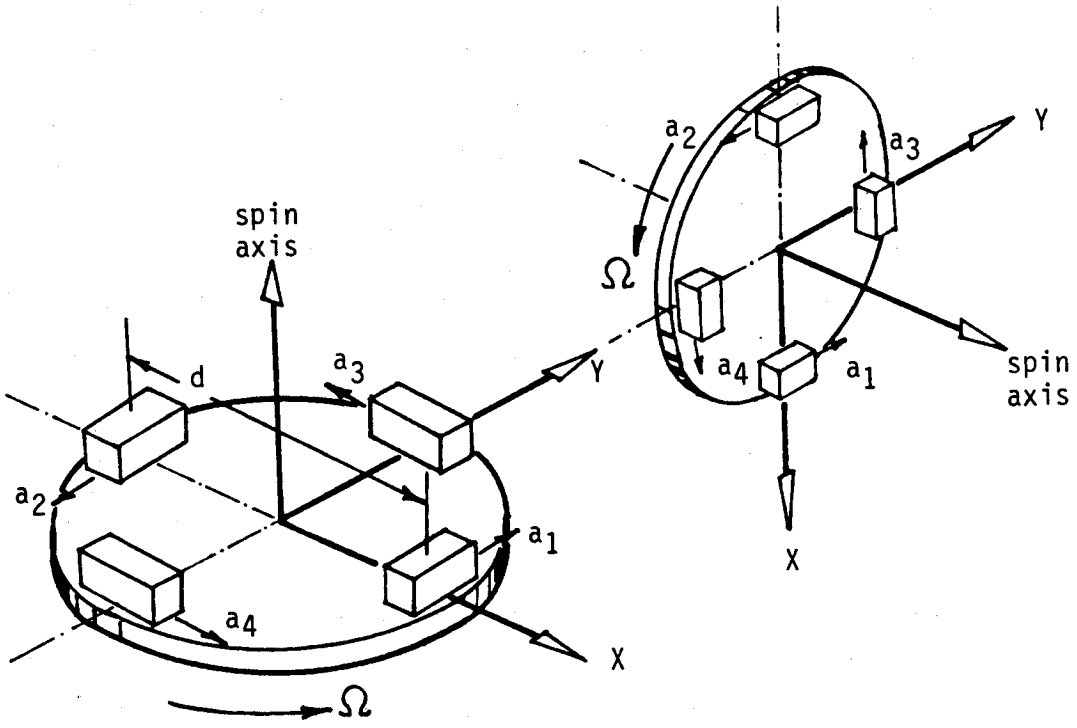

Figure 4. Operational concept of the Bell Aerospace gradiometer (from Wells, 1984, p.31).

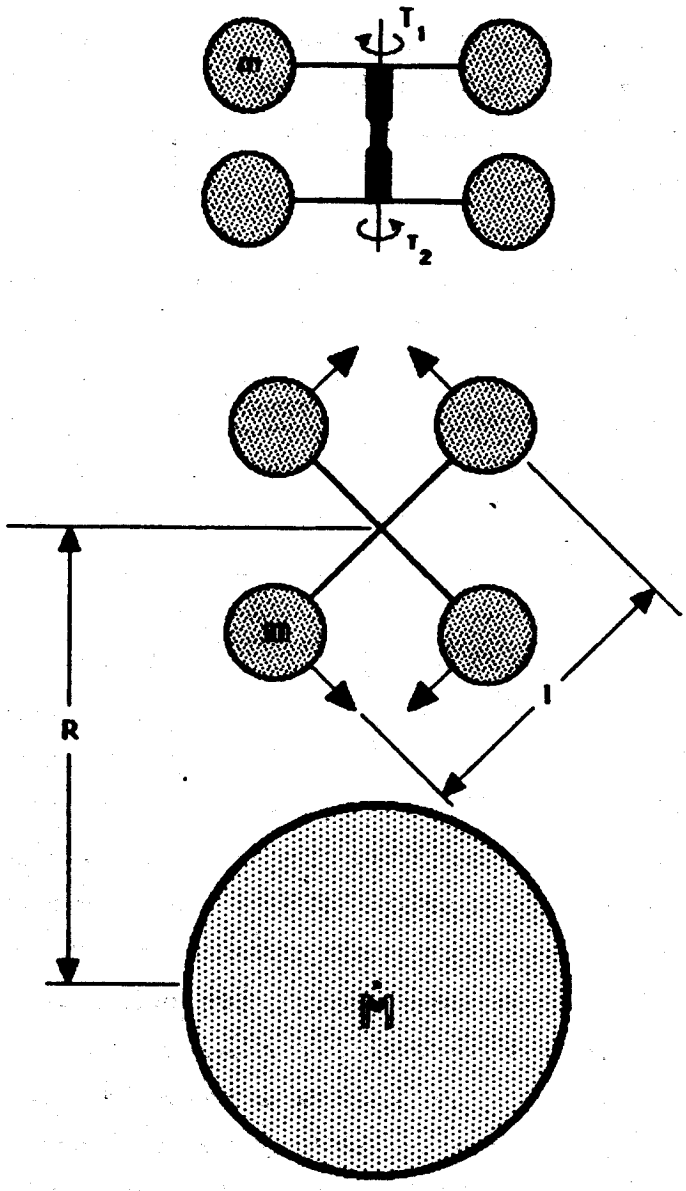

Figure 5. Operational concept of the Hughes gravity gradiometer (from Forward et al [1973]).

reported in Wells [1984] whether or not the system noise goal has been achieved.

The remaining organisations listed in Table 1 are developing cryogenic based gravity gradiometers, these are; Bendix/Stanford Univ., SAO/PSN, Sperry Defense Systems, and Univ. of Maryland. Brief descriptions and instrument sensitivity goals make up the remainder of this section.

The Bendix/Stanford University gradiometer utilizes superconducting Cavity Oscillator (SCO) technology developed at Stanford. The SCO is capable of detecting minute displacements on the order of 10^{-15} cm which it then converts to frequency form. Thus the output signal would be a frequency shift corresponding to the displacements experienced by a mass-spring accelerometer which are due to the gravity gradients. Bendix Field Engineering is developing the design of the SCO Based gradiometer. Their gradiometer, called the canonical gravity gradiometer, has six 3-axis SCO based accelerometers placed at distances of $\ell/2$ from the origin of a cartesian coordinate system (Figure 6). All nine components of the gravity gradient tensor can be approximated directly from the outputs of the 18 component measurements from the accelerometers. Recalling the definition of an Eotvos, the gravity gradient can be determined simply by differencing two accelerometer outputs and dividing by their along axis distances ($\ell/2$ or ℓ in the canonical case). The noise sources affecting the SCO based gradiometer have been investigated and it has been shown that a gradiometer with a sense mass of a few kilograms and a baseline of ½ m can have a resolution of 10^{-4}E over a 1 second sampling time (as reported in Wells [1984], p. 47). The primary error source for this sampling period is due to thermally induced vibration which is itself kept at a very low level since the instrument is operated at cryogenic temperatures.

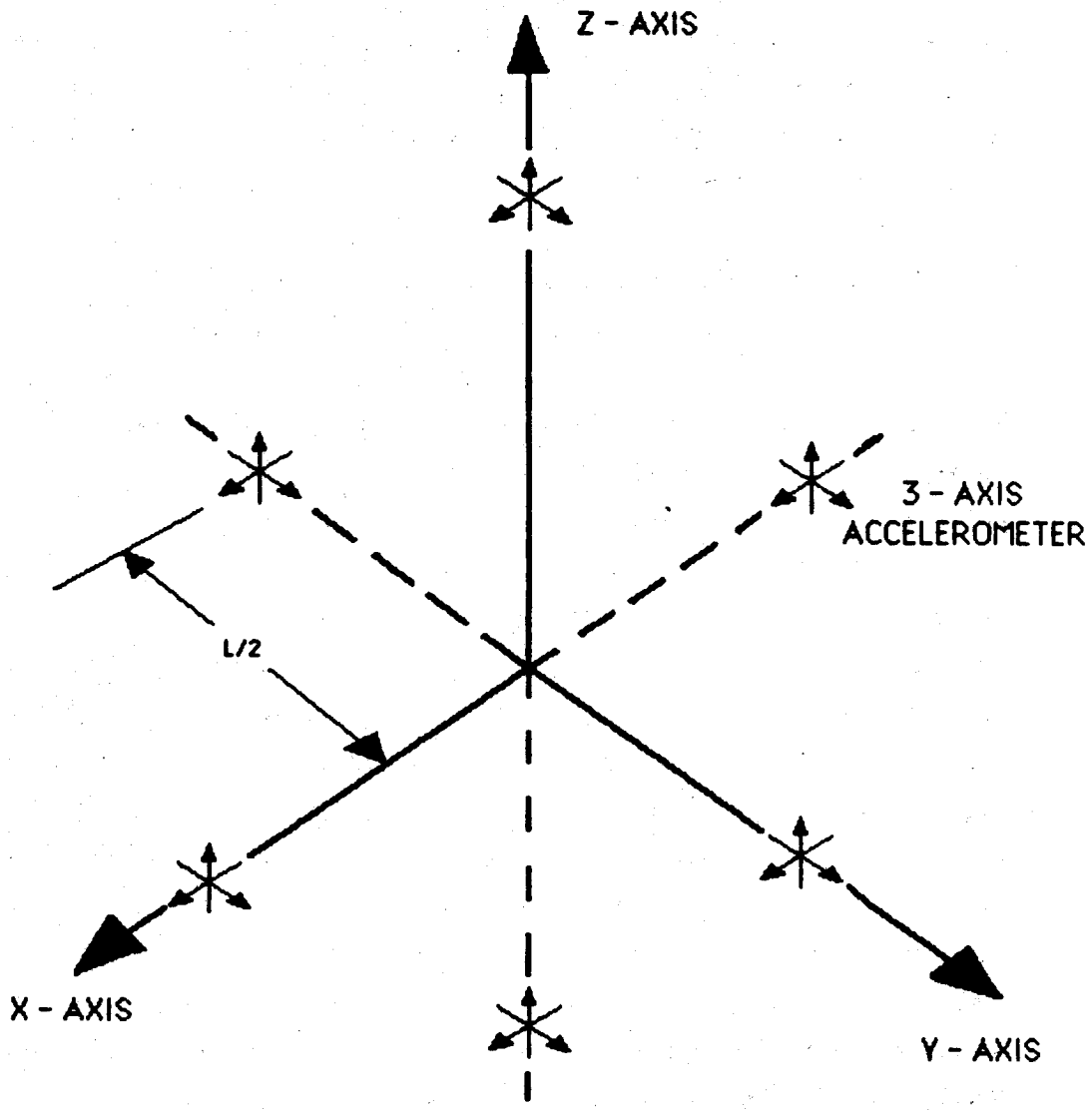

Figure 6. Canonical gravity gradiometer (from Wells [1984], p.43)

The Smithsonian Astrophysical Observatory (SAO)/ Piano Spaziale Nazionale (PSN) designs utilize gravity radiation antenna technology developed at PSN and cryogenic microwave cavity technology at SAO. The two approaches are being taken to determine which technology will be most suitable in a gravity gradiometer. Two single axis sensors are being constructed which will commence with the ultimate sensitivity goals of 10^{-2} to 10^{-3} E for the capacitive probe/radiation antenna gradiometer and 10^{-4} to 10^{-5} E for the cryogenic cavity gradiometer.

The gradiometer being developed by Sperry Defense Systems could be described as a cryogenic version of the Hughes design since they are related at least in principle. The Sperry design utilizes a magnetically levitated balance arm within a cylindrical bearing. The bearing itself is levitated and rotated at a constant rate such that the rotational rate is one half the natural frequency of the balance arm. The gradient signal is generated through the detection of inductance created by the rotating system. The detection is made by using a superconducting quantum interference device (SQUID) placed at the axis of rotation. A SQUID is a parametric device whose output voltage varies in response to an input flux. The cylindrical bearing responds only to angular accelerations which are transmitted to the balance arm (which is sensitive to the gradients as well). Thus a feed back loop can be established to null the effects of the angular accelerations by monitoring the bearing's angular position. In the orbiting instrument concept, the cylindrical bearing is replaced with a rotating sphere and an ensemble of three such spheres would be grouped in a noncollinear configuration to constitute the tensor gradiometer. Precise orientation and altitude determination are a requirement inherent in this design. The noise level goal set by the investigators at Sperry is 3×10^{-4} E.

Completing the list of active gradiometer developers is the design put forth by the University of Maryland. This design also uses SQUID technology to detect changes in the magnetic flux which is coupled to the displacement of a proof mass. Paik summarized the principles

involved very neatly in one sentence (Paik [1981]):

> "an acceleration Δg drives the proof mass to a displacement Δx, which is converted to a magnetic flux signal $\Delta \Phi$ by means of the superconducting inductive transducer and finally the magnetic flux is detected by the SQUID producing a voltage output ΔV."

The accelerometers can be placed in a configuration similar to that shown in Figure 6. When this configuration is used then the gradients are determined by differencing the outputs of the individual gradiometers following the concept underlying the definition of an Eotvos. In Paik [1981], ways of determining these differences are discussed and the concept of current differencing is introduced. Current differencing techniques provide a conceptually simple and efficient method to determine the in-line and cross gravity gradients. In the Univ. of Maryland design, the Niobium proof mass is weakly suspended which will limit gradiometry sensitivity to about 10^{-4} E over a 3 second integration time. Paik notes that the free-mass scheme would allow higher sensitivities and is realizable in space. Problems arise in attempting to test such a design in a "hostile terrestrial environment", i.e. the laboritory. Paik indicates further that a free-mass design in the zero-g evnironment of space could provide sensitivities up to 10^{-6} E.

In conclusion, it should be noted that cryogenic gradiometers promise higher resolutions than the conventional designs. However, the conventional designs for terrestrial and airborne applications are in a more advanced state of development. It should be noted too, though, that the latest push in gradiometric instrumentation is towards cryogenic designs and given enough time, with appropriate funding, cryogenic gradiometers could be available, in the next few years, for Earth gravity field determination as well as gravity missions to other terrestrial planets. This, then leads into a discussion of mission characteristics and proposed time tables.

2.3 Gradiometer Mission Characteristics

In this section, some aspects of mission and spacecraft design will be addressed. Many options exist at the moment and specific decisions are scheduled to be made over the next few years. Thus, only recommendations and assumptions will be made to delineate mission parameter limits to be used in the remainder of this study.

Since the principle objective of the gravity gradiometer mission is to obtain a global data set of gradient tensor values, the satellite should thus be placed in an orbit to facilitate global coverage. This is most easily done by placing the satellite in a polar orbit with the inclination angle to be as near to 90° as possible. Furthermore, as was mentioned in the introduction, higher resolution of quantities of interest (e.g. gravity anomalies) is acheived with lower altitudes. The atmospheric drag experienced by the satellite at these low altitudes becomes the primary factor for premature termination of the mission. Two approaches have been proposed. The first, as mentioned earlier, is the use of the Tethered Satellite System in which the instrument package with the gradiometer is lowered from the command vehicle (in this case the space shuttle) and measurements are taken. Three main disadvantages arize with this concept which limit its usefulness strictly to the gradiometer test phase. These are due to the inclination of the orbit, and duration of measurments, and untested tether dynamic models. The space shuttle normally operates in a relatively low inclination orbit (30°-50°) so that global coverage is impossible. The measurement density will likely be globally non-uniform due to the shortness of typical shuttle missions, which is undesirable from an analytical point of view. Finally, although investigations into the dynamic behavior of the tether systems are being made, the resulting models are largely untested in the real space environment. Until such tests are made, the gradiometer system's response to the tether's dynamic behavior remains uncertain.

The second aproach to overcoming the effect of the atmosphere for low orbits borrows technology from the GRM mission. In order to maintain an orbit at (say) 200 km altitude, it is necessary to compensate for the drag by employing thruster rockets. With a properly designed gradiometer, the accelerations from the thrusters will not affect the gradient outputs. It is this fact which causes gradiometers to be of interest in other dynamic applications (e.g. inertial navigation sytems, airborne and terrestrial gravity surveying). This thruster aided concept is formally called DISCOS (DISturbance COmpensation System). DISCOS, as used in the GRM mission, is under rather tight tolerances and constraints. For the gradiometry mission, the constraints can be eased somewhat, since it is not required that the gradiometry package be treated as a drag free proof mass, as is required in the satellite to satellite doppler tracking concept of GRM. It has been recommended that the free flying GGM mission utilize DISCOS technology or a variation of DISCOS. See Wells (1984), pages 59-60 for a more complete discussion.

Data coverage is a function of satellite inclination and altitude as well as of time. For the best distribution of data it would be advisable to avoid altitudes which yield resonant orbits with short period repeat cycles. The quality of distribution improves with longer mission durations. The optimal data distribution depends on the scientific goals of the mission. To guarantee that mission goals be met, it is advisable to overdetermine the system solutions (i.e. have too much data). However, mission planners must decide how much overdetermination is enough, given the economics of the mission. Also, in some cases, mission goals are relaxed. In this case it is easy to filter or smooth the raw data to meet these needs.

In Figure 7, the effects of varying mission durations can be seen. The data was generated with the same program as was used in the construction of Figures 1a and 1b. What it illustrates is that the recoverable ½°x½° mean gravity anomaly accuracy improves as the

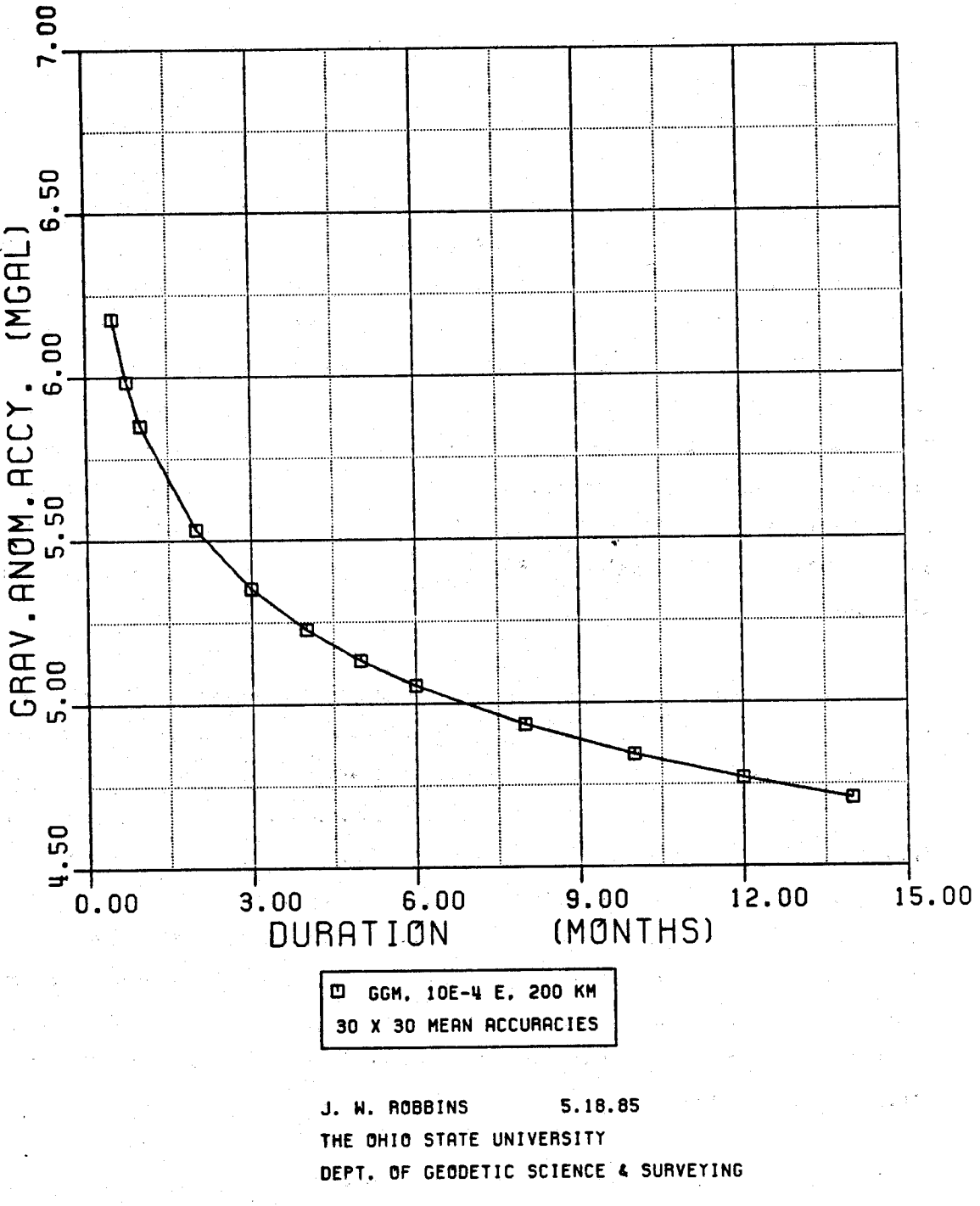

Figure 7. **30′x30′ mean gravity anomaly accuracies as a function of mission duration.**

duration increases (i.e. more data is available). It is quite easily seen that the curve levels off near 6 months and that a mission of twelve months only improves the mean gravity anomaly accuracy by approximately 5% in comparison with a six month mission. Thus it should be noted by system planners that extended missions may not realize significant improvements in determining static gravity anomalies.

The demands for satellite ephemeris and altitude monitoring will provide the designers of the autonomous mission some technical challenges. For example, the uncertainty in the attitude sensing system must not exceed $3x10^{-7}$ radians in order to prevent degredation of measurement precision. In constrast, the space telescope pointing requirement is an order of magnitude smaller, at less than $3x10^{-8}$ radians over a twenty minute observation period. It is expected that the attitude control and monitor problems can be overcome as mentioned in Wells [1984]. The design put forward by Paik [1981] should be capable of monitoring attitude and position directly by integrating certain gradiometer and accelerometer outputs. These integrated quantities can further be placed in an absolute reference frame by using state of the art conventional attitude sensors and tracking techniques.

It is necessary that certain assumptions be made concerning the parameters associated with an automomous satellite gravity gradiometry mission for the purpose of the primary investigation contained herein. These assumptions are outlined in Table 2. Using these parameters, then the raw data should be distributed every 4′ in latitude and every 3.6′ in longitude at the equator. The east-west spacing of the data decreases towards the poles due to the convergence of the orbits at the poles. The sensitivity of the instrument (10^{-3}E) was selected as a conservative estimate. Up to this point, the sensitivity goal of 10^{-4}E for the mission has not actually been achieved by any of the organizations developing gradiometers. The investigation scientists remain optimistic however, that sensitivity goals will ultimately be met.

Table 2.
Assumptions for Mission Parameters and Characteristics

* Mission parameters
  * Orbit - low eccentricity (circular)
    - inclination near 90 (polar)
    - altitudes of 200 km and 160 km
  * Duration - six months
  * Sample rate - 1 set of tensor measurements per second
* Instrument assumptions
  * Cryogenic full tensor gradiometer of the University of Maryland type
  * Sensitivity - 10^{-3} E (1 μgal km^{-1})
* Attitude and ephemeris assumptions
  * Data assumed to be corrected for attitude and attitude rates and converted from electrical output signals to real physical values
  * Data assumed to be rotated into local level cartesian coordinate system
  * Data assumed to be geographically tagged (latitude, longitude, altitude)

The particulars concerning the attitude and ephemeris assumptions are beyond the scope of this work but these assumptions will need closer examination after specific design decisions have been made. The rotation of the gravity gradients, from the orientation at the time of measurment to the local level coordinate system can be made by time tagging the gradient output signal and the absolute attitude information. The local vertical can be determined by the gradiometer output and the required rotation angles can be determined from the attitude information. The geographical tagging can be made by several methods

including integration of gradiometer outputs, supplemented with global positioning system (GPS) simultaneous phase measurements (described by Melbourne & Tapley [1983]) and other conventional tracking methods including laser and unified s-band radar tracking.

2.4 Previous Reduction Schemes

Several investigations have been made concerning techniques to reduce the satellite altitude gravity gradient measurements to some geophysically useful form. Two basic classes of reductions can be defined; global solutions and local solutions. The proposed global solutions attempt to determine the coefficients of the spherical harmonic expansion of the disturbing potential. The proposed local solutions attempt to determine directly, gravity quantities such as mean gravity anomalies and mean height anomalies (or mean geoid heights). A brief synopsis, highlighting certain aspects of these previously proposed solutions, follows.

Many gradiometer studies were made in the 1960's, however, most of these were proof of concept studies and dealt primarily with the improvement of inertial navigation system error sources. Geodetically relevant gradiometer studies began formal investigation in the early 1970's. Since then, the discussions have followed two paths; airborne gradiometry and spaceborne (satellite) gradiometry. Much work has been done for the airborne application and recent investigations by Jekeli [1985] illustrate the immediate usefulness of the airborne case. Although the airborne application and associated reductions will not be included here, it is important to recognize the close linkage between the two cases. The primary differences lie in the types of usable instrumentation and in the height of the gradient measurements.

One of the earlier investigations of satellite gradiometer data reduction appeared in a thesis by Glaser [1972]. In this work, Glaser proposed an algorithm which computes improved estimates of the

coefficients in the spherical harmonic expansion of the earth's gravitational field. Hence, Glaser's solution is of a global nature. It is very much a preliminary work as it was not possible for Glaser to fully test the algorithm. However, the proposed technique was novel for its time. Essentially, Glaser proposed that the measured gradients (from a rotating instrument) be downward continued to the earth's mean radius and then integrated to directly yield improved coefficients. Probably the factor most likely to have hindered Glaser's attempt at programming the algorithm was the considerable computational effort required. Even with the prospect of computational difficulty, Glaser's proposal, though very bold, set the starting point for further investigations.

That same year (1972), Reed outlined a reduction scheme which is less demanding with respect to the computations (Reed [1972]). Reed proposed a local solution where classical least squares techniques are used to determine 2°x2° and 5°x5° mean gravity anomalies referred to a 14x14 degree and order geopotential model. The results presented are in the form of an absolute error analysis, where the 2°x2° (and 5°x5°) mean anomalies predicted from the simulated gradients at altitude were differenced from the gravity anomalies used to create the simulated gradients. Reed was very perceptive in making investigations for both strap-down and rotating types of gradiometers, although his conclusions concerning the future of strap-down systems was faulty. Much of the present report draws from the analytical work of Reed.

The next definitive study on the geodetic usefulness of satellite gradiometry was made by Krynski and Schwarz [1977]. They were among the first to utilize the technique of collocation to compute geodetically relevant information from satellite gradiometry. In their study, they did work on determining the appropriate covariance model parameters, configuration of the gradiometer signals, and on combined solutions using additionally, terrestrial data. Their results, primarily in the form of a very generalized error analysis, yielded some fairly interesting conclusions. Among the more interesting of these is the

conclusion that only those gradients containing at least one radial derivative contribute significantly in recovering gravity information (in this case geoid heights). That is, only the T_{33}, T_{13}, and T_{23} gradients in the local level system contribute significantly. What appears to be missing from their study, however, is a discussion on the non-stationarity and anisotropic nature of the gradient covariances. Their conclusions remain sound in the case that their adopted covariance function behaves realistically.

Recently, a new attempt at the global solution has been outlined by Rummel & Colombo [1985]. Due to the remarkable breakthroughs in the computational methods of harmonic analysis on the sphere by Colombo, a new interest in large global solutions has resulted. Their proposed solution solves for the coefficients of the spherical harmonic expansion in an iterative process which includes orbit displacement and orientation uncertainties. A prerequiste for using the advanced analysis algorithm (decribed in elegant detail in Colombo [1981]), is that the measured data be in gridded form. Rummel & Colombo suggest creating cells of data averages which are then "dropped" onto a surface of revolution which better aproximates the actual orbits to create the gridded data set. By placing the data on an orbit approximating surface (rather than a sphere) helps to decrease the number of iterations required due to the reduction in the initial orbit displacement error. Rummel & Colombo ran computer simulations which showed, quite positively, the success of the method. There is much promise for this method because it has overcome many obstacles, notably the reduced computer time for the solution. The computer time required for the global solution is expected to remain substantial (i.e. greater than a few hours) thus, local solutions for direct gravity parameter recovery, such as the one outlined in this work, remain useful for those interested in regional investigations with a more direct approach (i.e. gravity gradients → gravity parameters rather than the three step method: gravity gradients → geopotential coefficients → gravity parameters).

3. APPLICATION OF LEAST SQUARES COLLOCATION

3.1 The Collocation Model

The techinque of least squares collocation has been used successfully for a wide variety of problems in physical geodesy. It has been especially useful in certain satellite mission applications such as in satellite altimetry (Rapp [1983]), satellite-to-satellite tracking (Hajela [1981]), and in estimating gravity potential differences between continents from satellite laser ranging data (Hajela [1983]). The results from these reports showed that significant solutions can be found with limited observational data. As is well known, for large observational data sets, the collocation technique suffers from the requirement that a large matrix be inverted or a large system of equations be solved. This drawback can be bypassed in two ways. First, the simpler approach is to determine what elements of the total data set can be ignored or which elements can be smoothed or averaged such that the errors resulting from the collocation soluton remain small. In this approach, one may be forced to accept some loss of resolution in order to reduce the computation time. The other method is to switch to frequency domain collocation where the inversion can be handled with less computational burden. Details of the latter technique are found in Eren [1980]. The present study will follow the former, more simple approach.

The fundamental equation of the least squares collocation technique is (Moritz, [1980], p. 102)

$$\hat{s} = C_{st} C_{\ell\ell}^{-1} \ell \qquad \text{(III.1)}$$

where ℓ is the vector of observations, $C_{\ell\ell} = (C_{tt} + C_{nn})$ is the sum of the covariances of the observations and the observational noise, C_{st} is the covariance matrix relating the observed quantities to the quantities being predicted, $\hat{S}$ is the vector of predicted quantities.

The observational noise is usually associated with the observed signal uncertainty and in most cases, this uncertainty is treated as uncorrelated from one observation to the next, thus the C_{nn} matrix will be diagonal with all the elements on the diagonal having similar values.

The collocation technique is especially appealing to geodesists since it allows for an estimate of the inherent error convariance matrix associated with the estimate vector $\hat{S}$. The error covariance matrix (E_{ss}) is found through (Moritz [1980], p. 105)

$$E_{\hat{s}\hat{s}} = C_{ss} - C_{st}C_{\ell\ell}^{-1}C_{st}^{T} \qquad \text{(III.2)}$$

where all quantites were defined above and, in addition, C_{ss} is the covariance matrix of the estimated signal. The diagonal of $E_{\hat{s}\hat{s}}$ provides the variance of the estimated quantities $\hat{S}$. In the case that only one signal is being predicted (i.e. $\hat{S}$ has only one element), then $E_{\hat{s}\hat{s}}$ will have only one element and this value will be the variance associated with $\hat{S}$.

Another aspect that makes collocation a desirable technique is due to the fact that various data types can be combined to yield perhaps more improve estimates of the quantities desired. This aspect will not be a factor in this study because the intention of this study is to examine one specific data type (i.e. gradiometry data).

3.2 Explicit Matrix Structure-Observation Vector

In the following discussion, the developments will be made in the most general way possible. This means that the "general case" corresponds to the case that all five independent gradient tensor components are used in the solution. If fewer components are used, as is the case in this investigation, it is not difficult to modify the following development to accomodate the changes.

The vector of observations, ℓ will then be composed, in the general case, of the five independent residual tensor component values determined at a particular location. To obtain these residual values, several preprocessing steps are required.

First, it is assumed that the instrument outputs have been converted to physical units and that these values have been rotated into the local level coordinate system. The angles required for the rotation are determined from the satellite attitude control subsystem. It is further assumed that the attitude information has a propagated noise level below that of which is detectable by the gradiometer, thus the rotation angles are assumed errorless. Once these preprocessing steps have been completed, then what results are the measured gravity gradients, shown as a "vector segment" below,

$$\begin{bmatrix} V_{33} \\ V_{22} \\ V_{12} \\ V_{13} \\ V_{23} \end{bmatrix}_{\{\bar{\phi}_i,\ \lambda_i,\ r_i\}} \qquad \text{(III.3)}$$

where the numerical subscripts denote the differentiation axes corresponding to Figure 4 and the quantities in braces are simply reminders that the measurements are position tagged with $\bar{\phi}_i$, λ_i, r_i being latitude, longitude, and radial distance from the geocenter for the

i^{th} observation respectively.

Grouping of the vector segments can be made in many ways, but for the purpose of gravity parameter estimation, the logical alternative is to group by geographic location. If the data is randomly distributed, it can be grouped by choosing the spherical distance ψ_o and including as segments in the observation vector, those gradient values at $\bar{\phi}_i$, λ_i such that

$$\cos^{-1}[\sin\bar{\phi}_p \sin\bar{\phi}_i + \cos\bar{\phi}_p \cos(\lambda_i - \lambda_p)] \leq \psi_o \qquad \text{(III.4)}$$

where $\bar{\phi}_p$ and λ_p are the latitude and longitude of the prediction point. However, using randomly distributed gravity gradient data causes problems in computing the required covariances. One way to overcome these problems is to grid the data in some fashion.

There are several data gridding schemes available and depending on the type of solution (i.e. global or local) some schemes may be excessively complex or simplistic for application here. The first step in gridding the data is to predict point gradient values at the grid intersections of a regional block (cf. Figure 12). A least squares collocation predictor could be used for this task where nearby gradiometer measurements are used as input to form the predicted values. Since the gravity gradients, as will be shown later, are a short wavelength phenomenon, the prediction should be based upon only those measurements that are sufficiently close enough to the predicted grid value to keep the loss of gravity information to a minimum. The grid values should be reduced to a specific surface in order to ease the covariance computational demands in the main collocation solution for gravimetric quantities. Moving the height dependent aspect of the gradient signal to the preprocessing step not only simplifies the computation of the covariances in the main collocation algorithm, but also

provides the possibility of forming the observation vector as will be described shortly. The reduction to the specific surface can be accomodated in the prediction step. The reducing surface assumed in this study is a sphere with a radius of R_M from the geocenter, which is equal to the average geocentric radii of the gradiometer measurements within the regional block. This surface should be sufficient in our case since the orbit is considered circular and we are considering observations in a relatively small region or block (with, in general, $\psi_0 \leq 5°$). Another such surface is a surface of revolution about the earth's axis which better fits the actual orbits (Rummel & Colombo [1985]). This surface is not used in this work because the radial uncertainties which are being solved for in Rummel & Colombo's global solution can be ignored in this type of solution without detracting from the overall results. It is also not used because of the complications resulting from the height dependent covariance computations. Thus, once these averages and reductions are made, then what results is a geographical grid of points, to each of which are attached the five predicted and reduced independent gradients shown in Figure 8.

The complete gradient vector is then structured from point 1 to point MN. In transposed form the gradient vector is

$$\ell^T = [V_{33}^1,\ V_{22}^1,\ V_{12}^1,\ V_{13}^1,\ V_{23}^1,\ldots,V_{33}^{MN},\ V_{22}^{MN},\ V_{12}^{MN},\ V_{13}^{MN},\ V_{23}^{MN}], \qquad \text{(III.5)}$$

where the superscripts indicate which point the gradient value pertains to. Thus the observation vector, for the case that all five independent tensor components are entering into the solution, will have 5(MN) elements. For the formulation used by Krynski & Schwarz [1977], only the three components containing at least one radial derivative enter into the solution. Thus their gradient vector had 3(MN) elements of the form

$$\ell^T = [V^1_{33},\ V^1_{13},\ V^1_{23},\ldots V^{MN}_{33},\ V^{MN}_{13},\ V^{MN}_{23}] \qquad \text{(III.6)}$$

For the usual case that the region considered is equi-angular, then $\Delta\bar{\phi}$ will equal $\Delta\lambda$ and M=N (in Figure 8). Equi-area regions should be used in the polar regions due to problems associated with the convergence of the meridians.

1	2	3	4	...	N-2	N-1	N
N+1	N+2	N+3	N+4	...	2N-2	2N-1	2N
2N+1	2N+2	2N+3	2N+4	...	3N-2	3N-1	3N
⋮	⋮	⋮	⋮	⋱	⋮	⋮	⋮
(M-2)N+1	(M-2)N+2	(M-2)N+3	(M-2)N+4	...	(M-1)N-2	(M-1)N-1	(M-1)N
(M-1)N+1	(M-1)N+2	(M-1)N+3	(M-1)N+4	...	MN-2	MN-1	MN

$\Delta\phi$

$\Delta\lambda$

Figure 8. Numbering scheme for gridded sub-blocks

To complete the observation vector set-up, the differences between the predicted grid gradient values and the computed reference gradients are taken to form the residual gradients (or anomalous gradients). This is done to meet the requirement that the observed data be centered. To center the data, reference point gravity gradients are computed for all components being considered in the solution at each point $(\bar{\phi}_i,\ \lambda_i)$ on the grid at radius R_M. The reference gradients are computed from a set of reference geopotential coefficients (C'_{nm}, S'_{nm}) complete up to degree and order N. The reference coefficients, together with $(\bar{\phi}_i,\ \lambda_i,\ R_M)$ are inserted into the properly differentiated version of equation (II.4). The differentiations were made by Reed [1972] and are summarized in Appendix A. Since the required reference gradients are on a grid, then advantage can be taken of the

mathematical symmetries which result, and a computationally efficient algorithm can be utilized, such as described by Robbins [1984]. The observation vector, ℓ can then be established by (cf. eq. (II.5))

$$\ell^i = \begin{bmatrix} V^i_{33} - U^i_{33} \\ V^i_{22} - U^i_{22} \\ V^i_{12} - U^i_{12} \\ V^i_{13} - U^i_{13} \\ V^i_{23} - U^i_{23} \end{bmatrix} = \begin{bmatrix} T^i_{33} \\ T^i_{22} \\ T^i_{12} \\ T^i_{13} \\ T^i_{23} \end{bmatrix} \quad (1 \leq i \leq MN) \qquad \text{(III.7)}$$

where ℓ^i is the i^{th} observation vector segment.

3.3 Explicit Matrix Structure - Covariance Matrices

The overall structure of the covariance matrices is dependent upon how the observation vector and the resulting signal matrix are structured. The basic structure of the observation covariance matrix will be 5MNx5MN, where MN are the total number of points contained in the NxM grid of locations. The matrix illustrated in Figure 9 will need to be inverted according to equations (III.1) and (III.2). Since the matrix is symmetric, some inversion computation time can be saved by storing the matrix in symmetric storage (vector) mode. However, for the purposes of testing and keeping computation times relatively short (less than 10 minutes on the IBM 3081 at the Ohio State University), the author selected 1000x1000 as the maximum dimension of the autocovariance matrix. If all five of the components are used (as shown in Figure 9), then, at a maximum, a grid of 200 points can be considered. This corresponds to a 14x14 grid of residual gravity gradient observations. More points on the grid can be utilized when fewer than five components enter into the solution.

The covariance matrix relating the observed quantities to the desired signal, C_{st}, has its structure defined through the number of

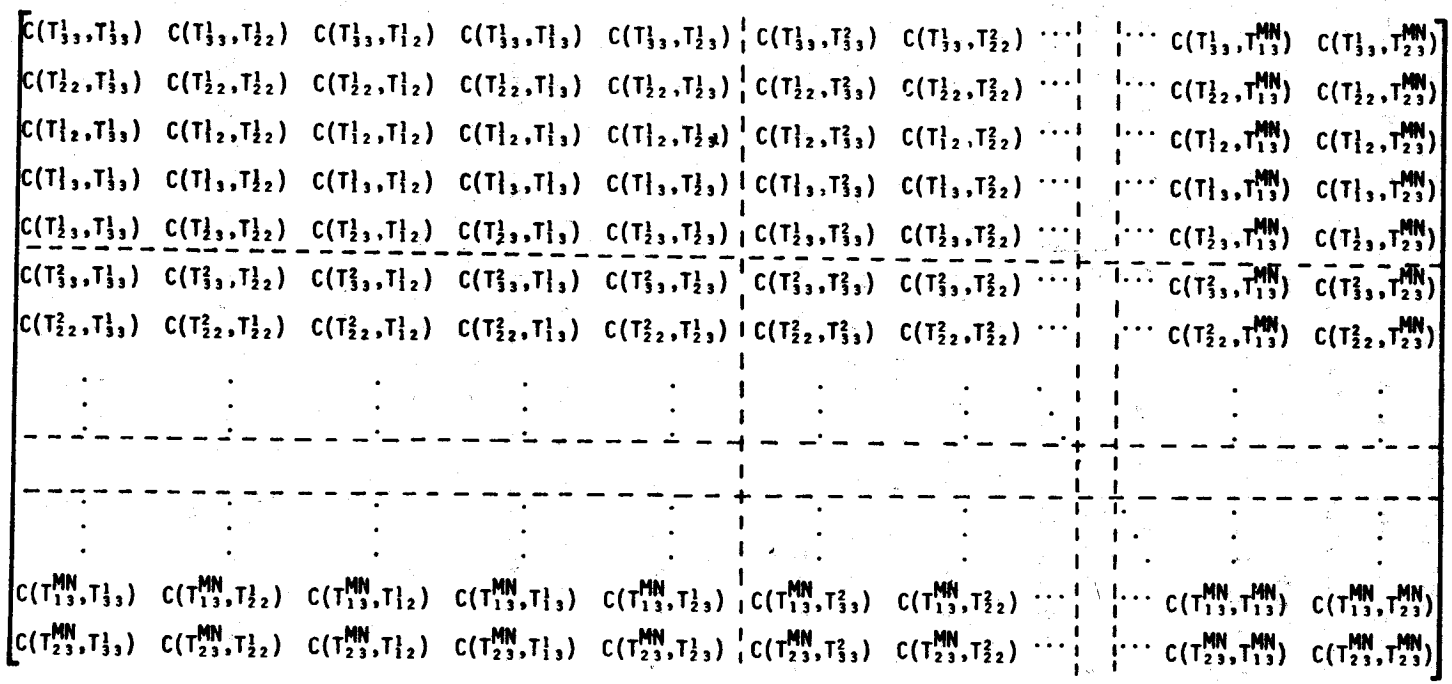

Figure 9. Observation covariance matrix structure.

observations and the number of predicted quantities. It will have the dimension L x 5MN where L is the number of predicted quantities and 5MN is the total number of observed gradients in the grid (general case). The predicted quantity can be any gravimetric quantity (e.g. gravity anomalies or height anomalies, as used in this study).

In general, C_{st} will be a row vector because normally only one quantity is being predicted. That is, only one gravimetric quantity, located in the center of the grid (and on the earth's approximating sphere), is computed for a specific grid. For adjacent predicted gravimetric quantities, the grid is shifted and observations symmetric to the computation point enter into the computation. Thus, a moving window technique is used in which the covariances are longitudinally invariant. Computation of the covariances themselves, follows.

3.4 Covariance Computations

The covariances associated with the gravity gradients as well as the gravimetric quantities can be expressed as linear functionals of the disturbing potential. This well known property contributes to the success of collocation. The general form for the covariances of the disturbing potential, T is

$$K(P, Q) = \frac{(GM)^2}{rr'} \left\{ \sum_{n=2}^{N} \left[\frac{a^2}{rr'}\right]^n (2n+1)\, \varepsilon_n^2 P_n(\cos \psi_{pp'}) + \sum_{n=N+1}^{\infty} \left[\frac{a^2}{rr'}\right]^n (2n+1)\, \sigma_n^2 P_n(\cos \psi_{pp'}) \right\} \qquad \text{(III.8)}$$

where r, r′ are the radial distances to point P and Q respectively, $\psi_{pp'}$ is the spherical angle separating P and Q, a is the mean equatorial

radius, and P_n are the Legendre polynomials of degree n. Furthermore,

$$\varepsilon_n^2 = \sum_{m=o}^{n} (\varepsilon^2\bar{C}_{nm} + \varepsilon^2\bar{S}_{nm})/(2n + 1) \qquad \text{(III.9)}$$

with the absolute error of the modeled coefficients given by

$$\varepsilon\bar{C}_{nm} = \bar{C}_{nm(true)} - \bar{C}'_{nm(model)} \qquad \text{(III.10a)}$$

$$\varepsilon\bar{S}_{nm} = \bar{S}_{nm(true)} - \bar{S}'_{nm(model)} \qquad \text{(III.10b)}$$

Since $\varepsilon\bar{C}_{nm}$ and $\varepsilon\bar{S}_{nm}$ are unknown, then as an approximation, the coefficient standard deviations of a spherical harmonic geopotential model solution, $e\bar{C}_{nm}$ and $e\bar{S}_{nm}$ are substitued for $\varepsilon\bar{C}_{nm}$ and $\varepsilon\bar{S}_{nm}$. The corresponding term, σ_n^2 in the right hand side of (III.8) is the degree variance of the potential coefficients;

$$\sigma_n^2 = \sum_{m=o}^{n} (\bar{C}_{nm}^2 + \bar{S}_{nm}^2)/(2n + 1) \qquad \text{(III.11)}$$

This formulation is originally due to Colombo [1980] (section 3.2) but the notation of Hajela [1983] (also section 3.2) is used here. The potential degree variances are related to the anomaly degree variances by (Hajela [1983], p.17):

$$c_n = \gamma_o^2(n - 1)^2(2n + 1)\sigma_n^2, \qquad \text{(III.12)}$$

where γ_o is a mean value of gravity.

The anomaly degree variances, c_n, are usually given by empirically derived models. Many collocation studies have used the Tscherning &

Rapp model:

$$c_n = \frac{\alpha(n-1)}{(n-2)(n+B)} \qquad \text{(III.13)}$$

where α and B are model parameters. The main reason for its extensive use is due to the availability of advanced software based upon this model (see Tscherning & Rapp [1974], Tscherning [1976], and Sunkel [1979]). This model exhibits logarithmic behavior and as such, it is not the most suitable model for certain types of covariance modeling. It has been especially criticized for its unreasonably high gradient variance especially in association with the parameters determined by Tscherning & Rapp (1974). These parameters were determined by least-squares fitting the model, equation (III.13), to observed anomaly degree variances from degree 3 to 20, 1° and 5° mean (block) anomaly variances, and a point variance of 1795 mgal^2. More recently, attempts to update the parameters were made by Rapp [1979], and Jekeli [1978] attempted using various other parameters to determine their effects on the variances of several gravimetric quantities (including the vertical gravity gradient). The specific parameters and the effects upon gradiometry solutions will be discussed in the next chapter.

Other models for the anomaly degree variance have been proposed by several investigators, we mention only the two component-model attributed to Moritz. It's basic form is

$$C_n = \alpha_1 \frac{n-1}{n+A} S_1^{n+2} + \alpha_2 \frac{n-1}{(n-2)(n+B)} S_2^{n+2} \qquad \text{(III.14)}$$

where the α_1, α_2, S_1, S_2, A, and B terms are the model parameters. Parameter investigations were made by Jekeli [1978], Hein and

Jochemczyk [1979], and Rapp [1979]. Although it has been shown by these investigators that more natural anomaly and gradient variances can be obtained from the two component model, this study will restrict itself, with regard to the analysis, to the Tscherning and Rapp model for the afformentioned reason of readily available advanced software. The results contained herein might be improved by using the two-component model.

The particular covariances are derived through the law of covariance propagation. The gravimetric quantities, i.e. gravity anomalies and geoid heights are related to the disturbing potential by (Moritz [1980], p.108)

$$\Delta g = - \frac{\partial T}{\partial r} - \frac{2}{r} T \qquad \text{(III.15)}$$

$$N = \frac{1}{\gamma_o} T \qquad \text{(III.16)}$$

with γ_o being a mean value of gravity. Both equations are given in spherical approximation. The functionals relating the gradients in a local level coordinate system to the disturbing potential are slightly more complicated. The functionals for the tensor diagonals are (Reed [1972], p.32);

$$T_{11} = \frac{1}{r^2 \cos^2\bar{\phi}} T_{\lambda\lambda} - \frac{\tan\bar{\phi}}{r^2} T_{\bar{\phi}} + \frac{1}{r} T_r \qquad \text{(III.17a)}$$

$$T_{22} = \frac{1}{r^2} T_{\bar{\phi}\bar{\phi}} + \frac{1}{r} T_r \qquad \text{(III.17b)}$$

$$T_{33} = T_{rr} \qquad \text{(III.17c)}$$

The sum of the above expressions yields Laplace's equation in spherical

coordinates. The off diagonal tensor functionals are:

$$T_{12} = T_{21} = \frac{1}{r^2\cos\bar{\phi}} T_{\lambda\bar{\phi}} + \frac{\tan\bar{\phi}}{r^2} T_{\lambda} \qquad \text{(III.18a)}$$

$$T_{13} = T_{31} = \frac{1}{r\cos\bar{\phi}} T_{\lambda r} - \frac{1}{r^2\cos\bar{\phi}} T_{\lambda} \qquad \text{(III.18b)}$$

$$T_{23} = T_{32} = \frac{1}{r} T_{\bar{\phi}r} - \frac{1}{r^2} T_{\bar{\phi}} \qquad \text{(III.18c)}$$

Now applying the law of covariance propagation with L_i and L_j denoting the functionals, the covariance of particular interest is (Moritz [1980], p.87)

$$M_{ij}(P, Q) = L_i^P L_j^{P'} K(P,Q) \qquad \text{(III.19)}$$

where K(P, Q) is given by (III.8). Substituting the functionals in (III.15) through (III.18) into (III.19) will yield all of the covariance types required in the "general case solution". These expressions have been derived by the author and are given in Appendix B.

It should be emphasized however, that in some cases, the resulting covariance expressions are no longer isotropic. That is to say, they are no longer strictly functions of the radial distances, r and r′, and the spherical distance, ψ_{PQ}. The gradient covariances can be treated in a manner similar to the treatment of vertical deflection covariances described by Tscherning & Rapp [1974]. Recently, Krarup & Tscherning [1984] have recast the T_{13}, T_{23} and T_{12} gradient component covariances into isotropic form for use in collocation solutions utilizing torsion balance observations. Tscherning has further modified his closed form covariance algorithm (COVAX) to impliment the isotropic form (Tscherning

[1983]).

3.5 Reduced Forms of the Collocation Solution

Since Krynski & Schwarz [1977] concluded that the gradients contributing significantly to the local collocation solution are those containing at least one radial derivative, then the "general case" of utilizing all five of the observable gradients can be reduced to utilizing the three radially differentiated gradients (T_{33}, T_{13}, T_{23}) with negligible loss of accuracy. If the same number of grid points is retained as was used in the consideration of the "general case" solution, then the computational burden and necessary computer time will be reduced especially for the inverson of $C_{\ell\ell}$. In this case, the observation vector will be

$$\ell^i = \begin{bmatrix} V^i_{33} - U^i_{33} \\ V^i_{13} - U^i_{13} \\ V^i_{23} - U^i_{23} \end{bmatrix} = \begin{bmatrix} T^i_{33} \\ T^i_{13} \\ T^i_{23} \end{bmatrix} \quad (1 \leq i \leq MN) \qquad \text{(III.20)}$$

where ℓ^i indicates the i^{th} observation vector segment with i being a number associated with a set of observation on a grid and where MN is the total number of points in the grid (cf. Figure 8). The observation covariance matrix will be similar to that shown in Figure 9 but without the T_{22} and T_{12} related covariances. The dimension of $C_{\ell\ell}$ is, in this case, 3MNx3MN and if it is again assumed that the maximum dimension of practical inversion for the purpose of testing is 1000x1000, then the grid can be enlarged to the size of 18x18. The enlargement can be made by densifying the grid (of specific geographic coverage) or by retaining the data density and extending the geographical coverage.

The formulation and covariance computations are simplified further by only considering the second radial derivative component (the vertical gravity gradient, T_{zz}). The covariance function for the vertical gravity gradient is isotropic from the start since the radial derivative functional, when applied to the anomalous potential covariance through the covariance propogation law, does not disturb the isotropic nature of the anomalous potential covariance function, K(P, Q) (cf. equation (III.19)). Only one observational type needs to be considered therefore only one autocovariance table needs to be generated. The observation covariance matrix will have dimension MNxMN and with the assumed maximum dimension of 1000x1000, then the grid can be further enlarged to 31x31. Again, either the density of observations can be increased (to a limit not to exceed the actual measurement distribution) or the geographical coverage can be made more extensive than for the case mentioned in the previous paragraph.

4. RESULTS OF THE ERROR ANALYSIS

4.1 Description of the Investigations

The investigations reported herein are primarily in the form of an error analysis. This is due to the fact that at this time, a satellite gravity gradiometer mission has not yet been tested, so no real data yet exists. The basis for the error analysis comes from the expression of the error covariances (equation (III.2)) which is repeated here for reference (cf. section 3.1 for term definitions),

$$E_{\hat{s}\hat{s}} = C_{ss} - C_{st}C_{\ell\ell}^{-1}C_{st}^{T} \qquad \text{(IV.1)}$$

This way the errors of the predicted signals are found by the model implied covariances, which are used to form the matrices C_{ss}, C_{st}, and C_{tt}, and the instrument noise level which enters through C_{nn} (recall that $C_{\ell\ell} = C_{tt} + C_{nn}$).

The original idea was to impliment the "torsion balance version" of Tscherning's COVAX program to compute the covariances for those gradients containing at least one radial derivative. However, the results of this attempt proved unsatisfactory either due to the instability of the inversion of $C_{\ell\ell}$ or due to undetected software errors. Thus to simplifiy the investigation, it was decided that only gradient components with two radial derivatives would be used as the assumed observable (referred to as the radial-radial component, T_{33}, in the remaining discussion).

The remainder of this chapter will include a discussion on the generation and behavior of the covariances, and presentations of the error analysis with variations in the parameters.

4.2 Covariance Generation and Behavior

Several methods have been devised to generate covariance tables. Two of the more popular methods are by truncated series and by closed form expressions. The truncated series method has been used occasionally with the two component degree variance model of Moritz (equation (III.14)). The closed form expression method has been programmed by Tscherning and Rapp [1974] and further modified by Tscherning [1976] and [1983]. The degree variance model used in the closed form expression has traditionally been that Tscherning & Rapp (equation (III.13)), however recently the Moritz model has been implimented in a closed form algorithm by Hein [1981].

The closed form algorithm of Tscherning [1983] has been used throughout the present work. This algorithm (referred to as COVAX in this report) was selected since it was readily available to the author and since it is easily adaptable for the use of higher order reference potential models.

The selection of parameters for use in the Tscherning & Rapp degree variance model poses an interesting problem. The parameters computed by Tscherning & Rapp [1974] implied a horizontal gradient variance of $3500E^2$ which is considered unrealistically high. The gravity anomaly variance of 1795 $mgal^2$ implied by their parameters has been accepted for several years but recently the value has come under close scrutiny. Evidence from studies of gravimetric quantities and empirical covariances in Canada have suggested that the 1795 $mgal^2$ value may be too high. For the Canadian region, Schwarz & Lachapelle [1980] estimated the gravity anomaly variance to be 837 $mgal^2$. One must

remember though, that the Canadian evidence is of a regional nature and thus it is limited to an incomplete set of gravity anomaly producing geophysical structures (i.e. the samples taken in Schwarz & Lachapelle's investigation do not include a global set of geophysical structures such as deep ocean basins, trenches, island arcs etc.). Thus their result for the gravity anomaly variance may be somewhat low, perhaps not by a very large amount. The horizontal gradient variance was estimated to be approximately $200E^2$ in Canada by Schwarz & Lachapelle which is in fair agreement with slightly higher gradient variances determined by Hein & Jochemzcyk [1978] in Germany. Therefore, the best degree variance model parameters to use are those which imply a global anomaly variance of approximately 1100 $mgal^2$ (Rapp, private communication) and a horizontal gradient variance of approximately 300 E^2 (as a compromise value between the results of Schwarz & Lachapelle and Hein & Jochemzcyk). One set of parameters for the Tscherning & Rapp degree variance model meets these variance requirements, which were determined by Jekeli [1978]. These parameters, as well as other used in previous investigations, are listed in Table 3 (cf. equations (III.13) and (III.14) for the expressions of the degree variance models). To illustrate the power spectrum of the three parameter sets of Table 3, the products of the degree variances with their respective S-terms are plotted by degree in Figures 10a and 10b. This product will be called the scaled degree variances and are found by

$$\bar{c}_n = c_n S^{n+2} \qquad \text{(IV.2)}$$

$$\bar{g}_n = g_n S^{n+3} = \frac{(n+2)^2}{R_E} c_n S^{n+3} \qquad \text{(IV.3)}$$

with c_n given by the Tscherning & Rapp model (equation (III.13)) and with g_n denoting the vertical gradient degree variance. For the Moritz two component model, the scaled degree variances are

$$\bar{c}_n = c_n \quad (c_n \text{ from equation (III.14)}) \tag{IV.4}$$

$$\bar{g}_n = \frac{(n+2)^2}{R_E}\left[\alpha_1 \frac{n+1}{n+A} S_1^{n+3} + \alpha_2 \frac{(n-1)}{(n-2)(n+B)} S_2^{n+3}\right] \tag{IV.5}$$

The variances are found through the summation

$$C_0 = \sum_{n=2}^{\infty} \bar{c}_n \tag{IV.6}$$

$$G_{ov} = \sum_{n=2}^{\infty} \bar{g}_n \approx 2G_{0H} \tag{IV.7}$$

with the last approximate equality shown by Jekeli [1978].

Figure 10a illustrates the scaled gravity anomaly degree variances for the three parameter sets of Table 3. The numbers associated to the curves correspond with the enumeration in Table 3. It can be seen that the Tscherning & Rapp model with Jekeli's parameters exhibits lower power than the other two models for degrees below 800 this is the reason for the lower value of the gravity anomaly variance, especially in view of (IV.6). Also notable, is the similarity between the Jekeli parameter model and the Moritz with Hein parameter model beyond degree 800. Tscherning & Rapp's parameters exhibit greater power for the high degree spectrum. All curves can be seen to exhibit high power at degrees below 700.

Figure 10b illustrates the scaled vertical gradient degree variances for the same parameter sets. The effects due to the two components of

Table 3. Degree Variance Model Parameters

1. Used in this work: Tscherning & Rapp model with Jekeli parameters

   α = 343.3408 mgal^2

   B = 24

   S = 0.9988961

   Implied variances:

   (Co: gravity anomaly variance, G_{0H}: horizontal gradient variance.)

   Co = 1089.5 mgal^2

   G_{0H} = 338.9 E^2

2. Tscherning & Rapp model with Tscherning & Rapp parameters:

   α = 425.28 mgal^2

   B = 24

   S = 0.999617

   Implied variances:

   Co = 1795 mgal^2

   G_{0H} = 3500 E^2

3. Moritz two component model with Hein [1981] parameters:

   α_1 = 7.516922 mgal^2 α_2 = 82.04054 mgal^2

   S_1 = 0.994425 S_2 = 0.9996642

   A = -2 B =7

   Implied variances

   Co = 1800 mgal^2

   G_{0H} = 1000 E^2

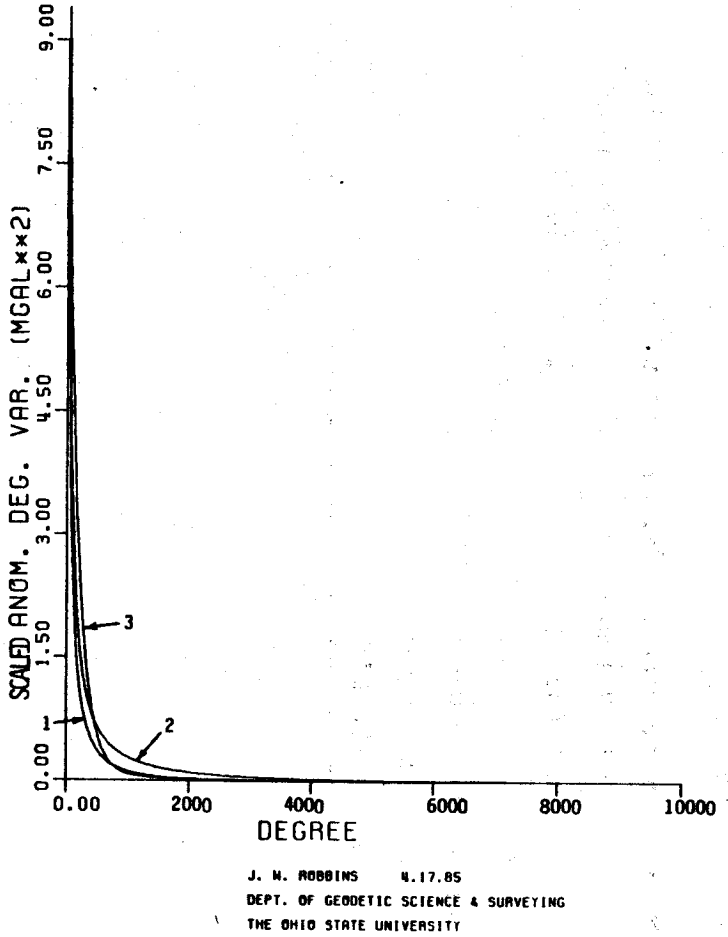

Figure 10a. Scaled gravity anomaly degree variances implied by the three parameter sets of Table 3. 1: Jekeli parameters, 2: Tscherning & Rapp parameters, 3: Hein parameters.

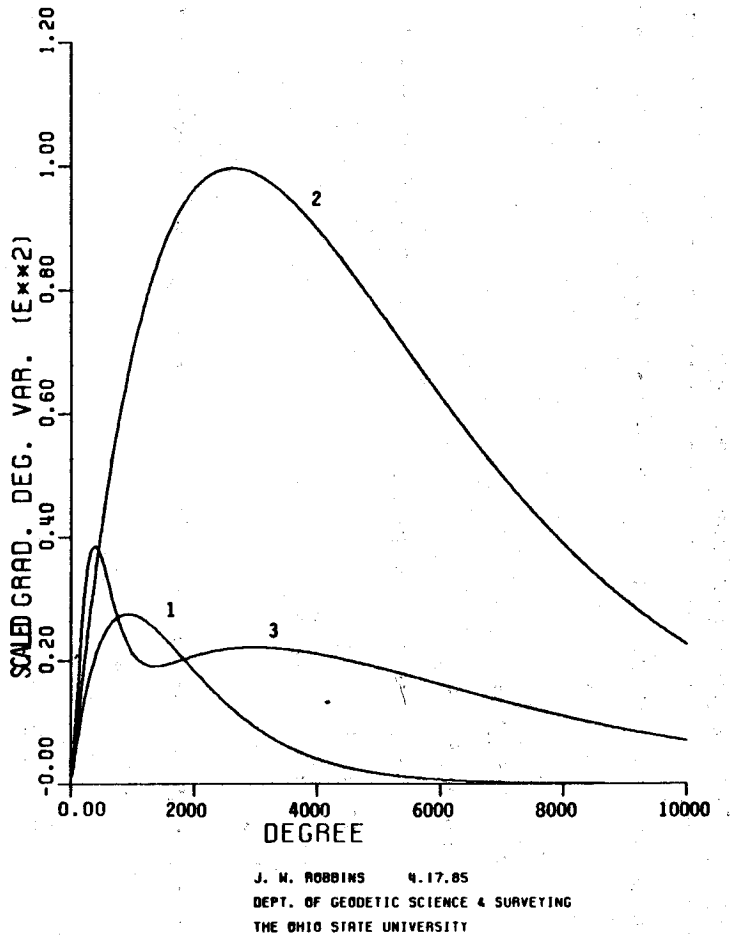

Figure 10b. Scaled vertical gravity gradient degree variances implied by the three parameter sets of Table 3. The numbering scheme is the same as Figure 10a.

the Moritz model are strikingly evident by the two maximums reached at n=390 and n=3000. The rather sharp maximum at n=390 is due to the logarithmic portion of the two component model. The two parameter sets based upon the Tscherning & Rapp model display similar spectral behavior. It appears that the spectrum beyond (roughly) degree 500 contributes to the high horizontal gradient variance implied by Tscherning & Rapp's parameters. Again, all curves exhibit the well known fact that gravity gradients are primarily a high degree (short wavelength) phenomenon. It should be remembered that the real world spectral behavior of the gravity gradient variance is still largely unknown. Perhaps with the influx of terrestrial and airborne gradiometry data, the parameters of the degree variance models can be refined further to incorporate this new information.

The effect upon the degree variances from using a high degree and order reference potential model to remove reference gravity gradients from the measured gradients is illustrated in Figures 11a and 11b. The DEC 81 reference potential model of Rapp [1981] has been selected for this purpose. Recall from Section 3.4 that the reference potential coefficient variances ($e^2\bar{S}_{nm}$, $e^2\bar{C}_{nm}$) are substituted for the indeterminable absolute error of the reference potential coefficients. Thus equation (III.9) becomes

$$\varepsilon_n^2 = \sum_{m=0}^{n} (e^2\bar{C}_{nm} + e^2\bar{S}_{nm})/(2n + 1) \qquad \text{(IV.8)}$$

The error potential degree variances are related to the error anomaly degree variances by

$$\varepsilon_c = \left[\frac{GM}{R_E^2} \right]^2 (n-1)(2n+1)\varepsilon_n^2 \qquad \text{(IV.9)}$$

The scaled error anomaly degree variances are found by substituting ε_C from (IV.9) for the C_n in (IV.2)

$$\varepsilon_{\bar{C}} = \varepsilon_C S^{n+2} \qquad \text{(IV.10)}$$

further, the scaled error vertical gradient degree variances are found by substituting ε_C for C_n in (IV.3)

$$\varepsilon_{\bar{g}} = \frac{(n+2)^2}{R_E} \varepsilon_C S^{n+3} \qquad \text{(IV.11)}$$

Figures 11a and 11b illustrates these scaled error degree variances implied by the DEC 81 coefficient degree variances. The DEC 81 degree variances are a modified set of degree variances not reported in Rapp [1981]. The degree variances used in this study were recomputed by (IV.8) up to and including degree 36. Beyond degree 36 the error potential degree variances were computed by the expression

$$\varepsilon_n^2 = e^2(\bar{C}, \bar{S})_n \qquad n>36 \qquad \text{(IV.12)}$$

where $e(\bar{C}, \bar{S})_n$ are approximate degree accuracy estimates given by

$$e(\bar{C}, \bar{S})_n = \frac{e(\Delta g)\theta}{2\gamma_o(n-1)\sqrt{\pi}} + \text{sampling errors} \qquad \text{(IV.13)}$$

where $e(\Delta g)$ is a global estimate of the accuracies of the 1°x1° mean gravity anomalies used in determining the coefficients; for the modified degree variance computation, a value of 10 mgal was used; θ is the

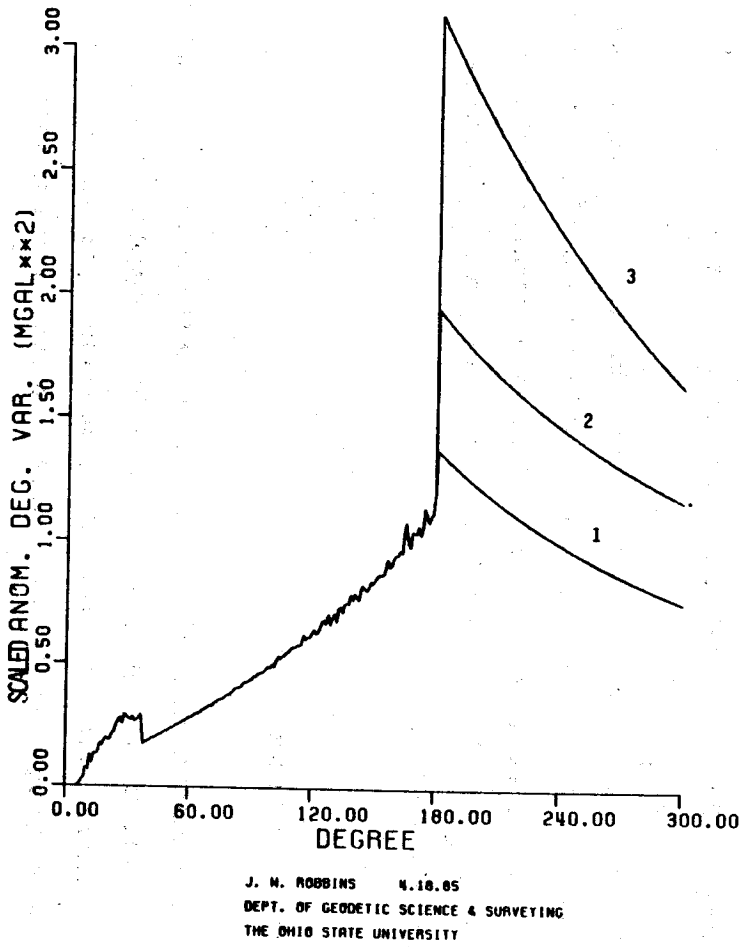

Figure 11a. Scaled error gravity anomaly degree variances implied by DEC 81 geopotential coefficient variances. Curves beyond degree 180 are gravity anomaly degree variances for the three parameter sets of Table 3. Numbering scheme corresponds to Figure 10a.

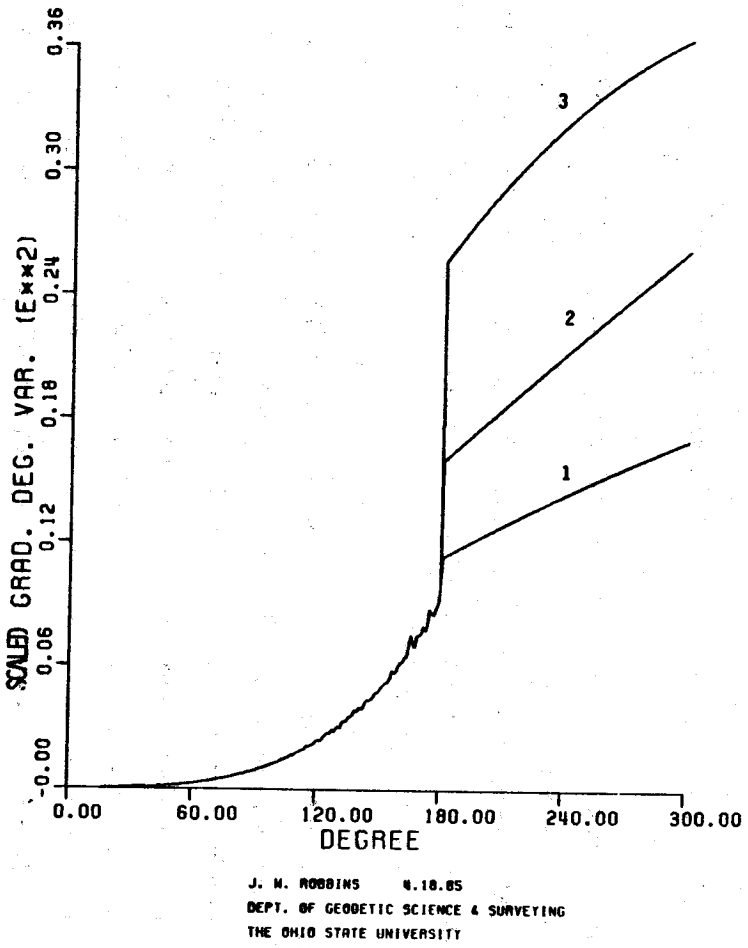

Figure 11b. Scaled error vertical gravity gradient degree variances implied by DEC 81 geopotential coefficient variances. Curves beyond degree 180 are vertical gravity gradient degree variances corresponding to Figure 10b.

block size (1°x1°, i.e. θ=1°), and γ_0 is a mean value of gravity.

The scaled degree variances belonging to the three parameter sets of Table 3 are shown in Figures 11a and 11b for n>180. It should be noted that the error degree variances abruptly alter the spectrum of the modeled degree variances. This is especially true for the anomaly degree variances of Figure 11a.

As geopotential models improve, their coefficient accuracies will improve further supressing the error degree variance influence in the covariance computations. As a minimum case, one can consider the reference geopotential model to be errorless (i.e. the coefficients are equal to the true coefficients in equation (III.10)). In this case (also considered in the next section), the degree variance spectrum has no power up to degree 180 and power beyond that degree as given by the empirical degree variance model. Considering the reference potential coefficients to be errorless is useful in determining the sensitivity of the resulting accuracy of the gravimetric quantities to the coefficient accuracies implied by the geopotential model actually used. A discussion of the results of this consideration is made in the next section.

To summarize, the covariance model of Tscherning & Rapp will be used for the remaining investigations due to its ease of operation and availability. The parameters of Jekeli [1978] were chosen to be the most compatible with the latest estimates of the gravity anomaly and horizontal gradient variances.

4.3 Results of the Error Analysis

The error analysis primarily consists of determining the expected error of the resulting gravimetric quantity computed through the collocation technique for an assumed geographic area at altitude. A computer program has been written which implements equation (IV.1) by

using covariances computed from the "torsion balance version" of COVAX by Tscherning. The program is called GIFRAD, for which a listing may be found in Appendix C.

There are three primary input variables for program GIFRAD, these being; the latitude, $\bar{\phi}$; the overall grid size, D; and grid spacing, DELD. The latitude is necessary for the computation of the spherical distances, equation (B.3) in the appendix, since the grid is to be based upon the lines of latitude and longitude. The overall grid size and the grid spacing are illustrated in Figure 12. These parameters can be varied which then offers the possibility for investigating the behavior of the error estimate with regard to these parameters. The gridded gradient values lie at the intersections of the grid lines, as shown in Figure 12, at a mean satellite altitude computed as described earlier in section 3.2. The gridded values of Figure 8 are treated as point values in Figure 12. The error analysis utilized an equi-angular grid, thus referring to Figure 8, $\Delta\lambda=\Delta\bar{\phi}$ and M=N, therefore in Figure 12, N=M=(D/DELD)+1. The value of M and N are constrained to be odd thus causing the central point of the grid to be positioned directly above the computation point, P. This causes a symmetric distribution of data which can be utilized to decrease CPU time during program runs.

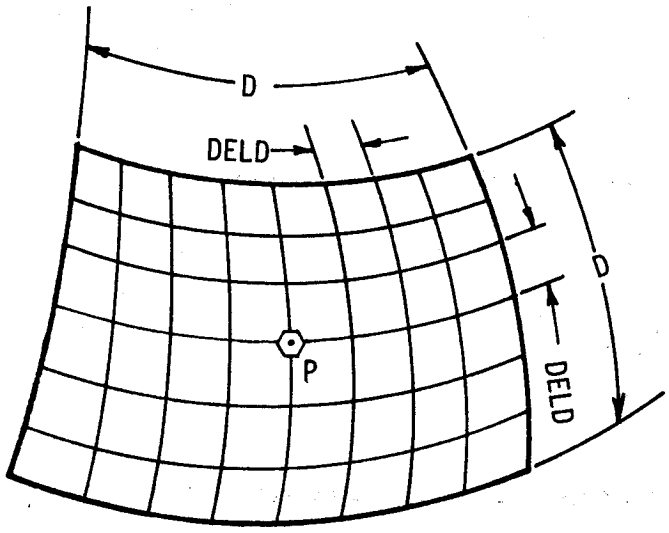

Figure 12. Grid size and spacing definition. D is the grid width and DELD is the grid interval.

The computed gravity and height anomaly accuracies are in terms of 30′x30′ means which correspond to a spatial resolution of approximately 56 km. Since mean values were chosen, the covariances must reflect this choice. Several methods have been devised to compute mean gravity quantity covariances. A good theoretical discussion can be found in Jekeli [1978], whereby the Pellinen smoothing operator is applied. However, a considerably simpler approach has been advanced in Tscherning and Rapp [1974] whereby the Pellinen operator is approximated by a height dependent quantity. Jekeli [1978] writes the mean gravity anomaly as

$$\mathrm{Cov}(\Delta\bar{g}_P, \Delta\bar{g}_Q) = \sum_{n=2}^{\infty} \beta_n^2 c_n S^{n+2} P_n(\cos\psi_{PQ}) \qquad \text{(IV.14)}$$

Tscherning and Rapp [1974] write, in the same notation, the approximate formula as

$$\mathrm{Cov}(\Delta\bar{g}_P, \Delta\bar{g}_Q) = \sum_{n=2}^{\infty} c_n \left[\frac{R_E^2}{(R_E+h)^2}\right]^{n+2} S^{n+2} P_n(\cos\psi_{PQ}) \qquad \text{(IV.15)}$$

Thus, the Pellinen operator, β_n^2 is approximated by

$$\beta_n^2 \approx \left[\frac{R_E^2}{(R_E+h)^2}\right]^{n+2} \qquad \text{(IV.16)}$$

Since the Pellinen operator is a function of the spherical distance ψ_0,

$$\beta_n = \frac{1}{1-\cos\psi_o} \int_{\cos\psi_o}^{1} P_n(t)dt \qquad \text{(IV.17)}$$

where $t=\cos\psi_o$, then it refers to the smoothing within a cap of the size ψ_o. However, block sizes of 30′x30′ are of interest, thus the corresponding cap size can be determined from

$$\psi_o = 2\sin^{-1}\left[\frac{\theta\sin\theta}{4\pi}\right]^{\frac{1}{2}} \approx \theta^{\circ}\pi^{-\frac{1}{2}} \qquad \text{(IV.18)}$$

where θ is the size of the block. Therefore when $\theta = 0.5^{\circ}$, then from (IV.18), $\psi_o = 16'56''$.

The value of the height, h which best approximates the β_n-function for $\psi_o = 16'56''$ is found by comparing the gravity anomaly variance computed from (IV.14) for the particular block size θ to the variance computed from (IV.15). Since, in the case of variance computations, P=Q, then the Legendre polynomial term becomes unity. Thus, the comparisons are based upon the following equations:

$$\mathrm{Var}_1(\Delta\bar{g}) = \sum_{n=2}^{N} \beta_n^2 c_n S^{n+2} \qquad \text{(IV.19)}$$

$$\mathrm{Var}_2(\Delta\bar{g}) = \sum_{n=2}^{N} \left[\frac{R_E^2}{(R_E+h)^2}\right]^{n+2} c_n S^{n+2} \qquad \text{(IV.20)}$$

where N is the maximum degree of the summation. The comparison was made by programming equations (IV.19) and (IV.20) with N=2000 by a

program called COVEQUIV. For the present investigation, the degree variances used were

$c_n = \varepsilon_c$ (from eq. (IV.9)) $\quad (2 \leq n \leq 180)$

c_n = Tscherning & Rapp model with Jekeli parameters $\quad (n > 180)$

The results of the comparison yielded a value for h of 6389 meters.

The covariances required in the radial/radial collocation solution were generated by COVAXX where the error anomaly degree variances implied by the DEC 81 geopotential coefficients, the parameters of Jekeli, and the height h associated with the mean gravimetric quantites were provided as input. The covariances, in table form, were placed in program GIFRAD where too, the input parameters D and DELD (cf. Figure 12) were specified. Another set of runs were made to test the effect of the geopotential model errors upon the resulting gravity anomaly and height anomaly accuracies. This was performed by means of omitting the coefficient errors in the covariance computations. This is equivalent to assuming a perfect geopotential field model. The variances of the predicted quantities (C_{ss} in equation (III.2)) area as follows: DEC 81 model errors included; 302.12 $mgal^2$ and 1.161 m^2 gravity anomaly and height anomaly variances respectively; perfect goepotential model to degree 180: 224.74 $mgal^2$ and 0.114 m^2 gravity anomaly and height anomaly variances respectively.

The final results of both sets of runs are illustrated in Figures 13a-13g. Using the above variances for the predicted quantities, it can be noted that the inclusion of gradiometer data causes a substantial improvement in the mean gravity anomaly and height anomaly accuracies. Four curves are associated with each figure with the curves having open box type symbols referring to gravity anomaly accuracies and

curves with cross type symbols referring to height anomaly accuracies. Note that the respective accuracy scales are plotted on each side of the figures.

Several observations can be made from the results. First, the accuracies improve with smaller grid intervals. This is not unusual since the number of geographical points increases as the interval, DELD decreases while the grid width D remains constant, that is, more data in entering into the solution. The accuracies would reach their minimum, for a specified grid width, when the grid interval becomes infinitely small, or in other words, if the gradiometry data were continuous over the region. However, this minimum cannot be achieved for two reasons: one, the dimension of $C_{\ell\ell}$ would become infinite, and two, continuous data is not realizable by current and planned gradiometers. Furthermore, the minimum grid interval is constrained by the mission parameters, most notable, the data acquisition rate, which determines the raw data geographical spacing, and by the assumptions concerning the gridding technique.

Noteworthy too, is the rather large jump in the accuracies for grid intervals larger than one degree when the coefficient uncertainties are included. This is a natural outcome of the spatial resolution of the reference model which is approximately one degree. Therefore, the poor accuracies resulting from the geographically sparse data distribution is due to the influence of the coefficient uncertainites. Note that the "errorless" accuracies retain a smooth character for grid intervals beyond one degree of arc.

The figures also indicate a general increase of accuracy as the grid width is increased for grid intervals less than one degree of arc. For instance, if one considers a specific grid interval (e.g. 30′), then as the grid width is increased two things are happening. First, more data is entering into the algorithm and second, the errors due to the omission of the region exterior to the grid are being reduced. Both are thereby

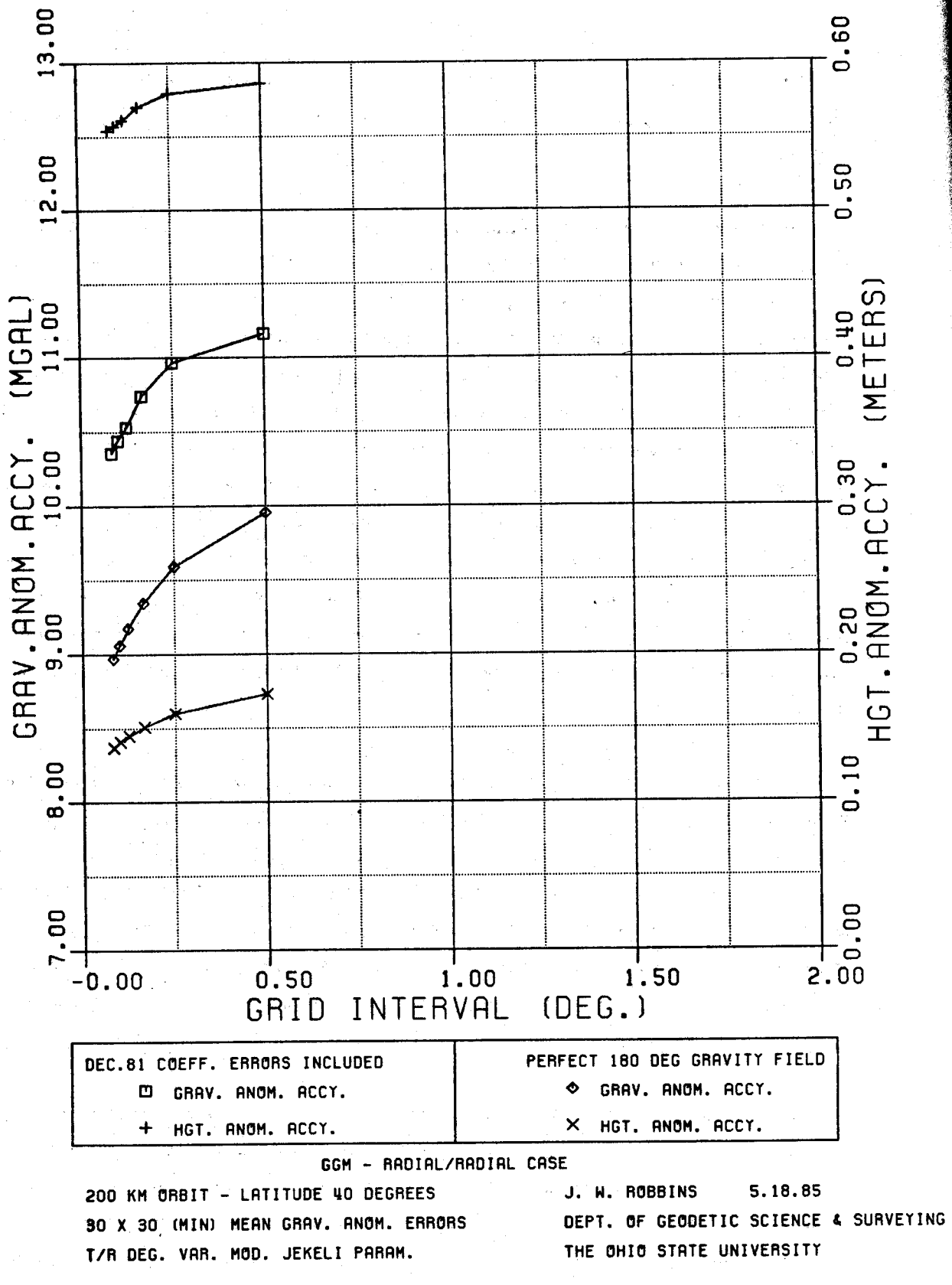

Figure 13a. 30′x30′ mean value (Δg, ζ) accuracy estimates for a 1° grid width.

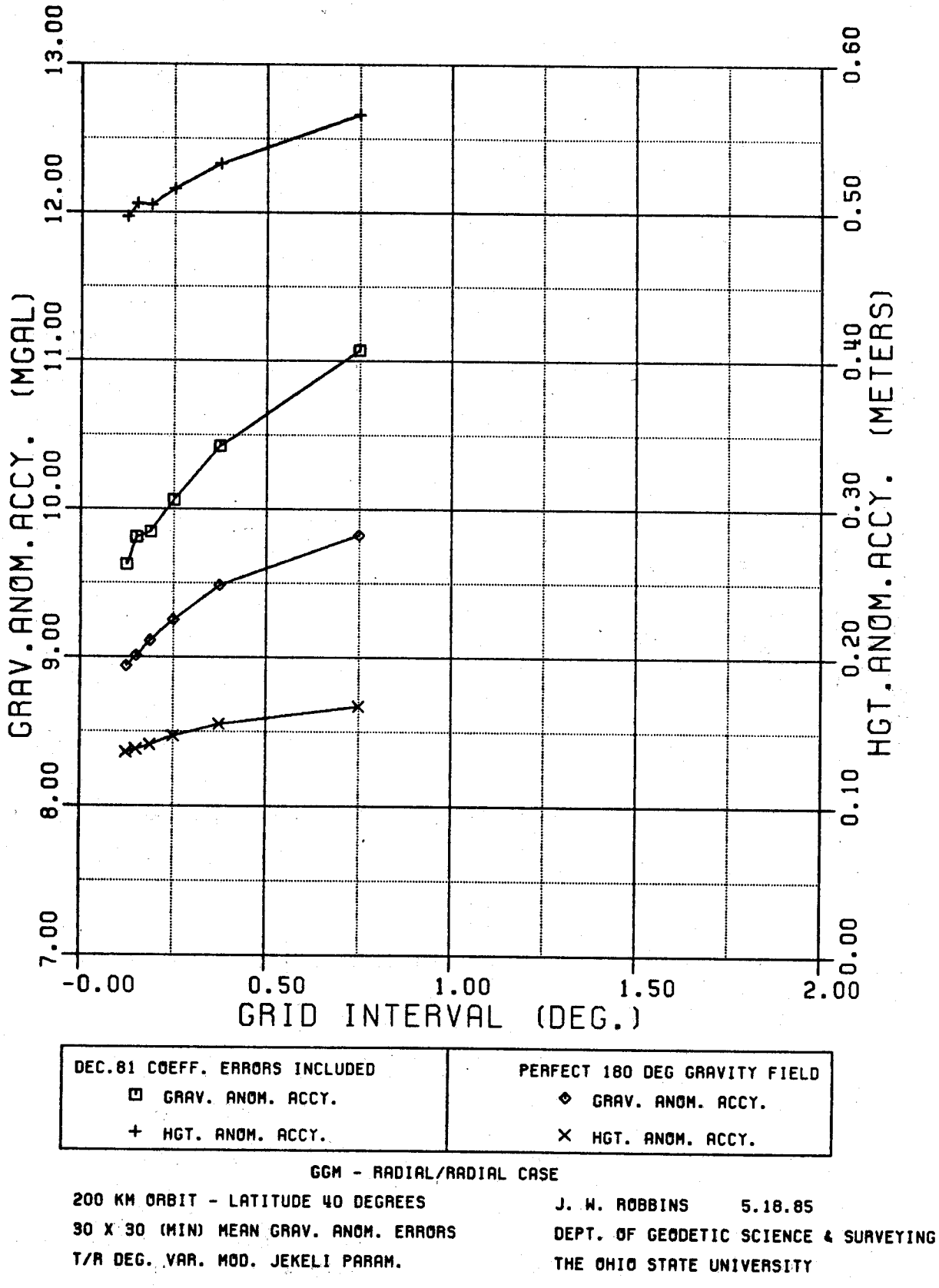

Figure 13b. 30′x30′ mean value (Δg, ζ) accuracy estimates for 1:5 grid width.

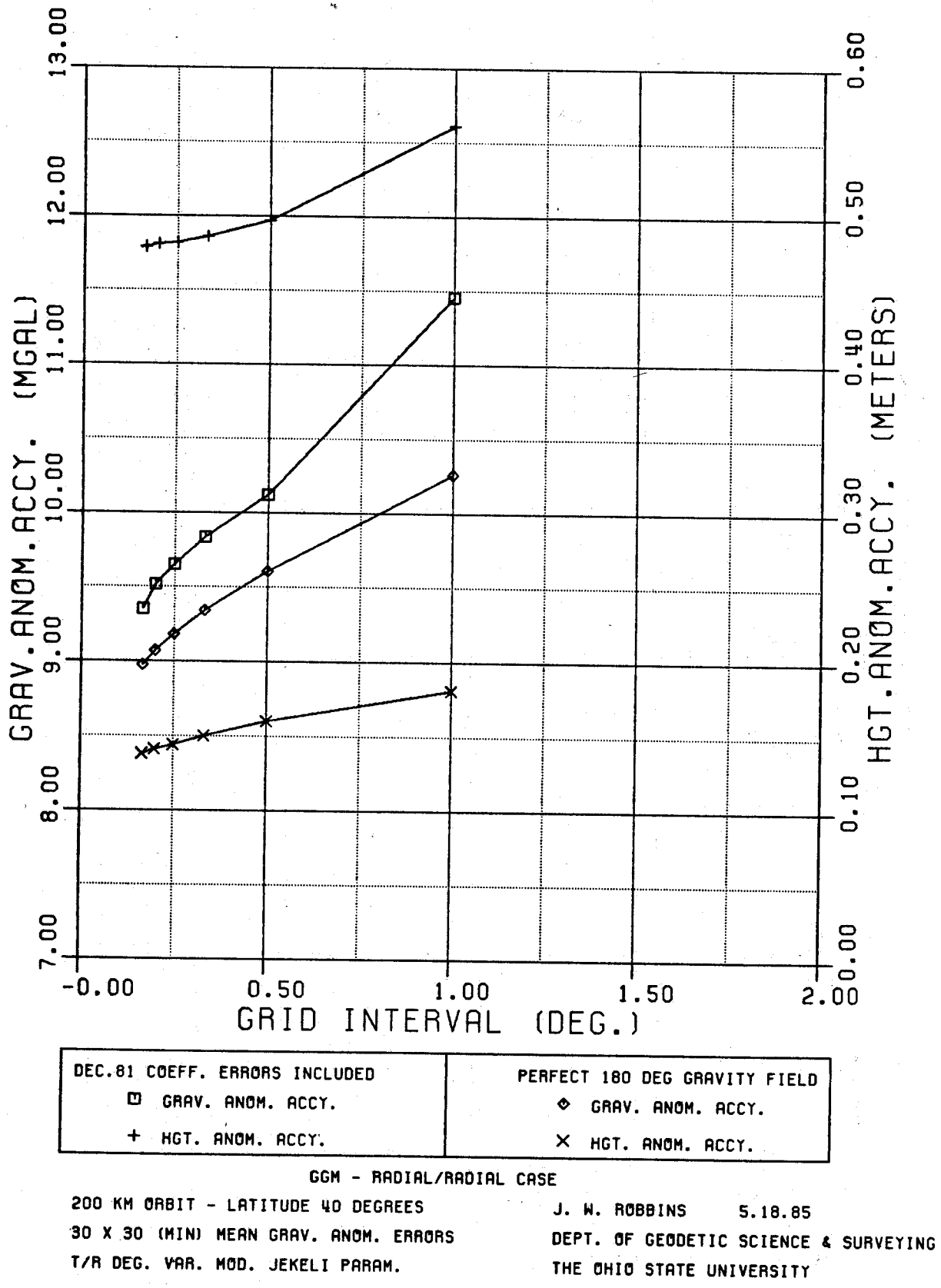

Figure 13c. 30′x30′ mean value (Δg, ζ) accuracy estimates for 2° grid width.

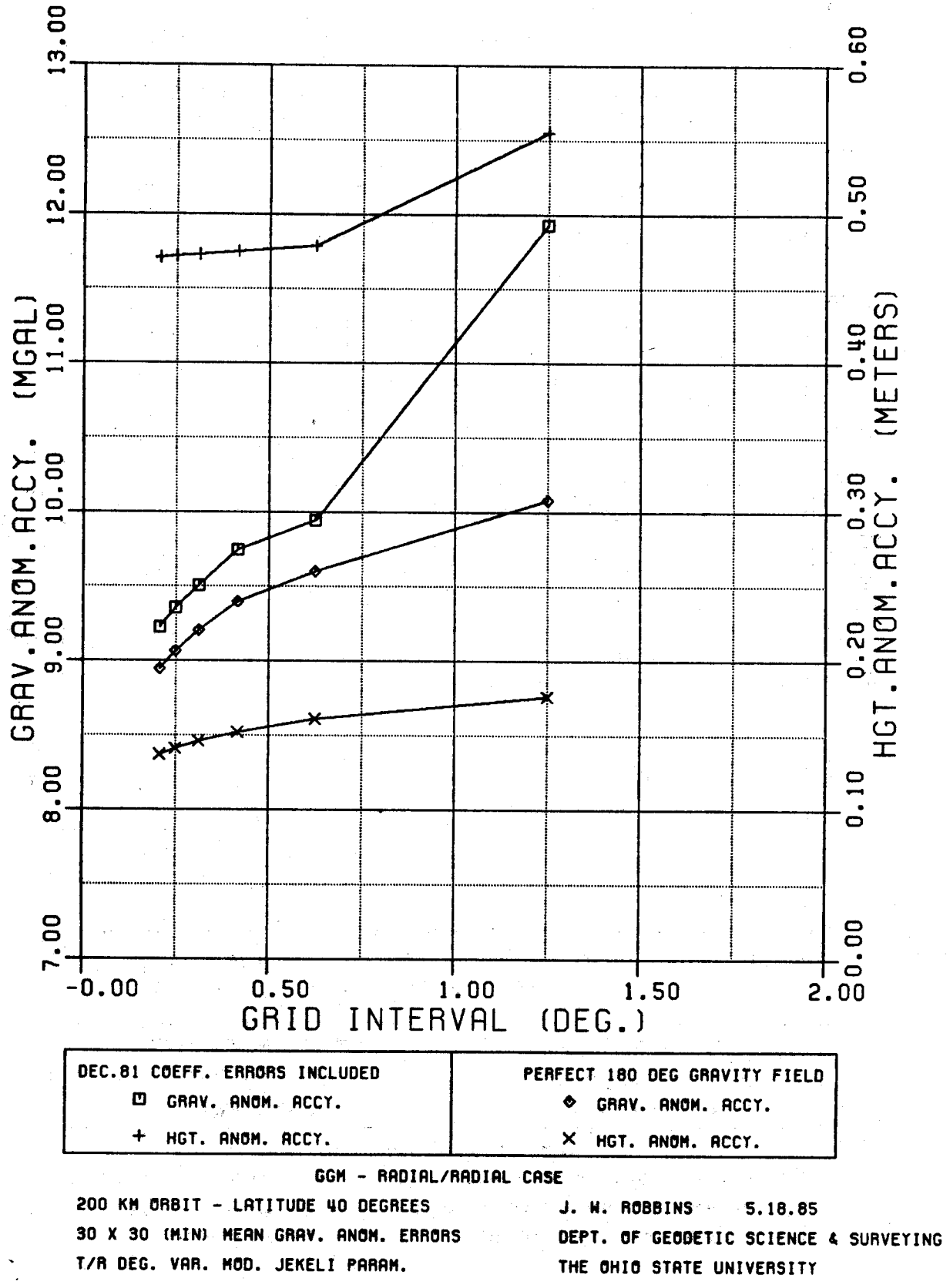

Figure 13d. 30′x30′ mean value (Δg, ζ) accuracy estimates for 2°.5 grid width.

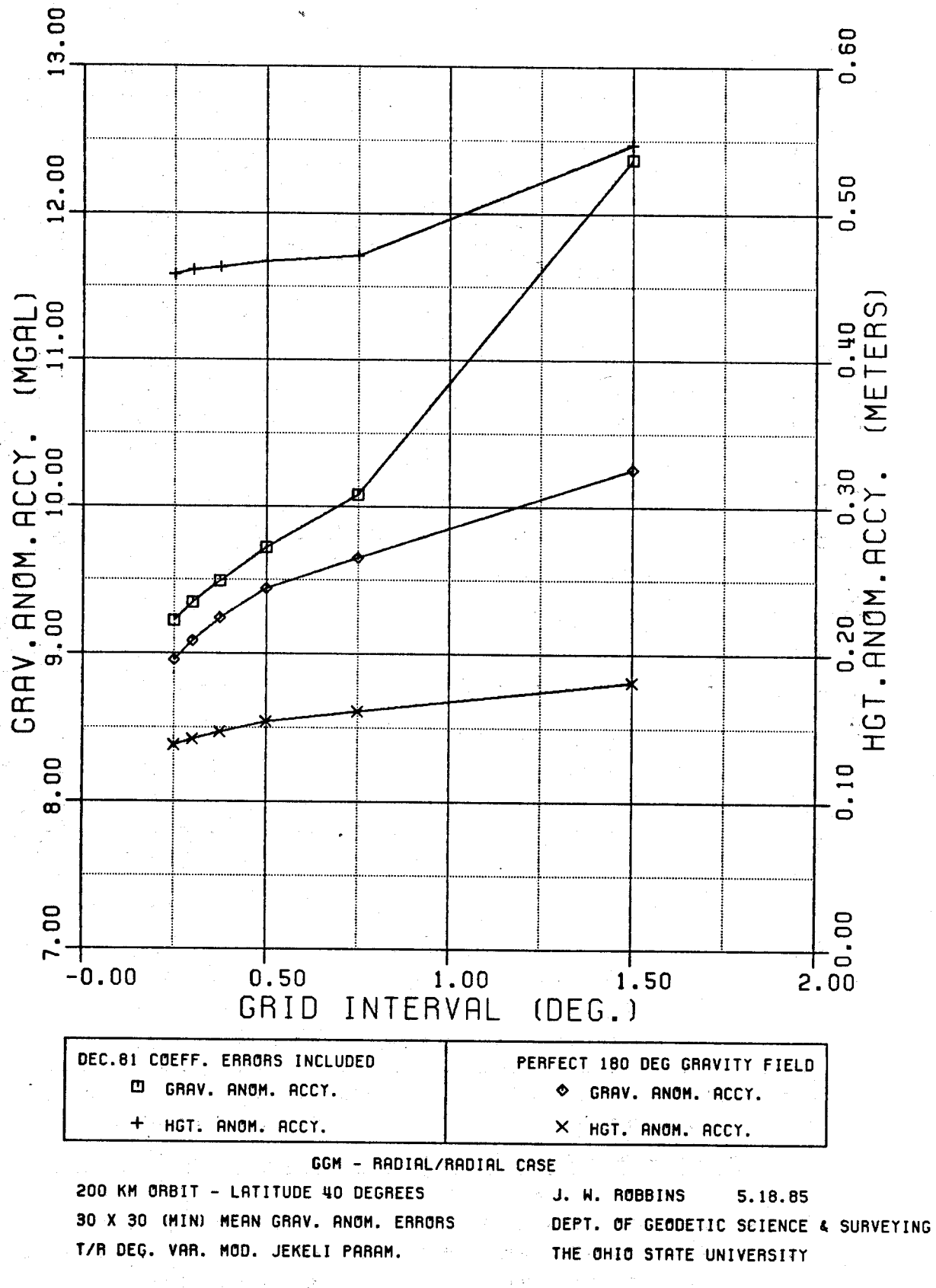

Figure 13e. 30′x30′ mean value (Δg, ζ) accuracy estimates for 3° grid width.

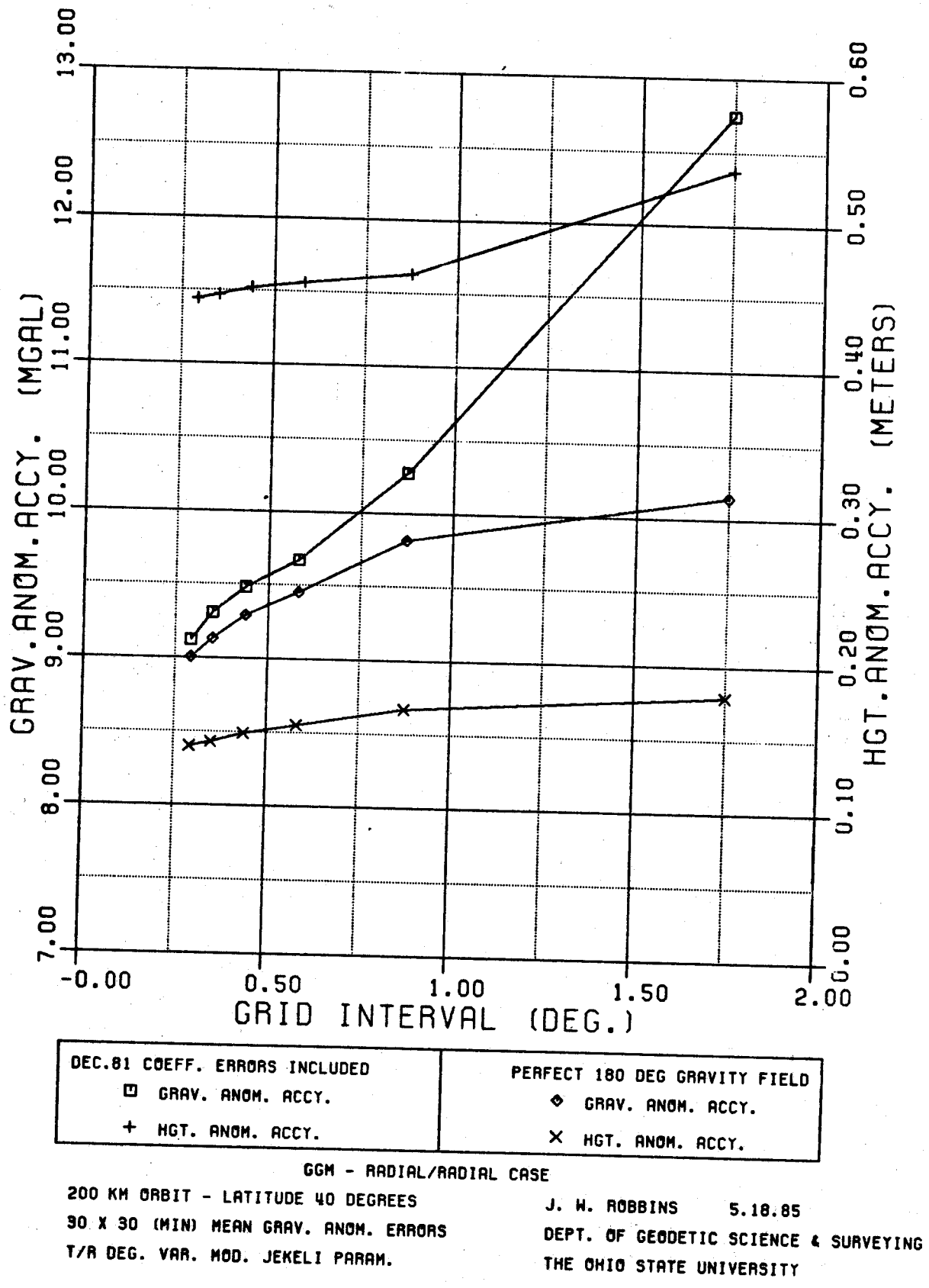

Figure 13f. 30′x30′ mean value (Δg, ζ) accuracy estimates for 3°.5 grid width.

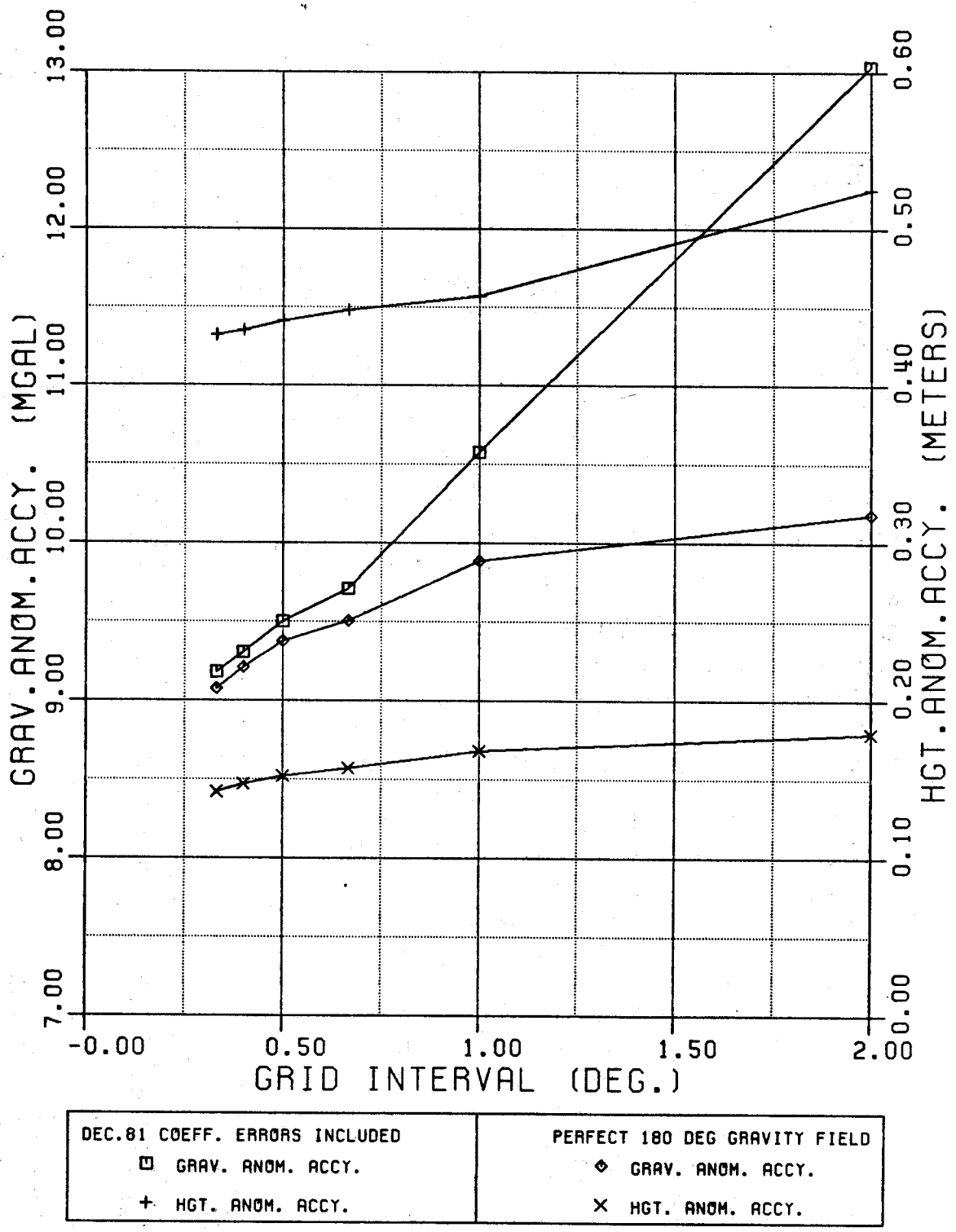

Figure 13g. 30′x30′ mean value (Δg, ζ) accuracy estimates for 4° grid width.

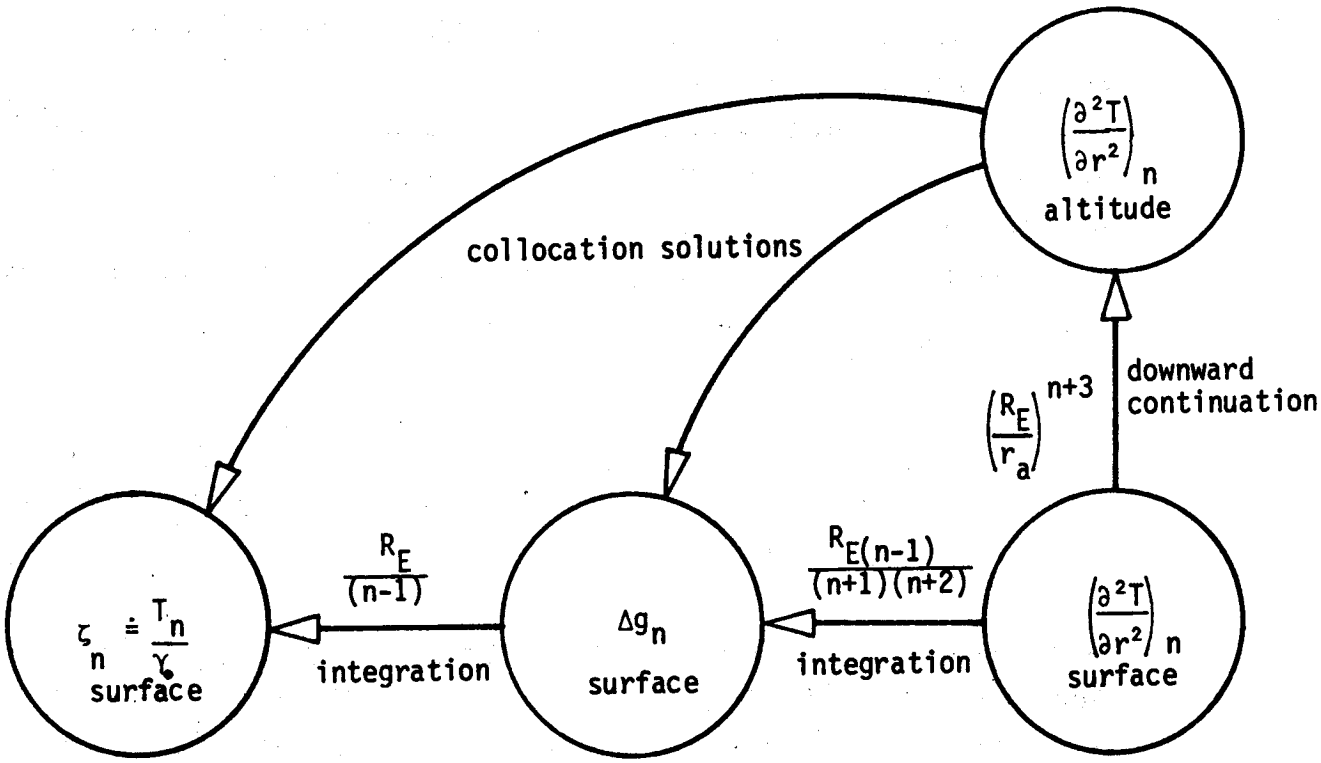

Figure 14. Relationship between gravity gradients and gravimetric quantities. Arrows point in direction of smoothing (damping of high frequencies) with spectral operators also shown. In the diagram, R_E is a mean earth radius, γ_o is a mean value of gravity at the earth's surface, and r_a is the radius of the satellite at altitude. From Rummel (1975).

effecting the accuracies, causing their improvement. It should be noted that the rate of accuracy improvement per increase in grid width can be seen in the figures to be decreasing as the grid widths are enlarged towards 2°.

Additionally, it should be noted that, in general, the mean height anomaly accuracy does not improve as dramatically as the mean gravity anomaly accuracy considered as a function of decreasing grid interval spacings (i.e. introducing more data into the algorithm). This is easily attributable ot the relationships between the mean gravimetric data dn the gridded gradiometric data (Figure 14). The tranformation from gravity gradients to gravity anomalies is functionally equivalent to an integration whereby smoothing takes place according to the spectral operators given in the figure. The situation is similar for the transformation from gravity anomalies to height anomalies. The transformation from gravity gradients is, in effect, undergoing two smoothings with a combined spectral operator of

$$\frac{R_E^2}{(n+1)(n+2)} \qquad \text{(IV.21)}$$

which behaves like $1/n^2$. Since in Figure 13a-13g, shorter wavelength data is entering into the solution when the data density is increased (by reducing the grid interval), then, from the spectral operators, it follows that the height anomaly accuracies behave smoother than the gravity anomaly accuracies since the operator (IV.21) suppresses the higher frequencies to a greater extent than the gradient-to-gravity anomaly operator

$$\frac{R_E(n-1)}{(n+1)(n+2)} \qquad \text{(IV.22)}$$

The accuracy estimates were computed for several other altitudes as given in Table 4. The overall improvement of the gravity anomaly accuracies is due to the strengthening of the signal in the medium wavelength gravity information. The accuracy will reach a minimum at a certain altitude which is a function of instrument sensitivity, data distribution and data coverage. The accuracies of the height anomaly changed only a negligible amount since the improvement of the gradient signal at lower altitudes occurs at frequencies higher than those which contribute the majority of the total height anomaly signal.

Table 4. 30′x30′ mean gravity anomaly accuracies computed by the local collocation algorithm GIFRAD for a grid width of 2¾° and a data spacing of 15′. Coefficient uncertainties included. Instrument sensitivity: 10^{-3} E at 40° latitude.

Altitude (km)	$\Delta\bar{g}$ accuracy (mgal)
200	9.36
180	8.60
160	7.61
140	6.96

Finally, the sensitivity of the accuracies to the coefficient errors can be clearly seen in Figures 13a-13g. Since the height anomalies are most affected by long wavelength information, they show marked improvement when the long wavelength error in the coefficients are removed. On the other hand, the gravity anomalies show only moderate improvement when the potential model uncertainties are removed. This behavior clearly indicates that a highly accurate geopotential model when used in the local collocation algorithm can significantly improve the resulting gravimetric accuracies. Since more accurate models will be available when the satellite gradiometer mission is launched, then for solutions using this algorithm, the resulting accuracies will be

significantly better than those reported here. As gravity models improve, the degree and order of their expansions will increase. This can also improve the accuracies of the resulting gravimetric quantities computed by this algorithm, if the uncertanties of the coefficients remain optimally small.

In summary, the primary investigation, in the form of a local collocation error analysis, has been described and complete results for a 200 km altitude gradiometer mission were presented with and without the influence of the DEC 81 coefficient uncertainties. The choice of degree variance model used in the study was made in lieu of available software and that the parameters of Jekeli adequately represent the actual gravity field in terms of the implied gravimetric variances. The effects of the DEC 81 geopotential coefficient uncertainties upon the degree variances were mentioned. It was noted that the error degree variances abruptly changed the power spectrum from its smooth character implied by the modeled degree variances and further, the minimum case of assuming errorless coefficients was described as a useful method to determine the sensitivity of the resulting gravimetric accuracies. The accuracy results were presented and their characteristics were discussed particularly with regard to data density, mission altitude, and reference coefficient uncertainty sensitivity. In the final chapter, comparisons to other results will by made along with concluding remarks.

5. DISCUSSION AND CONCLUSIONS

5.1 Comparison to other Investigations

It would be useful to place the results of this study in context with other similar investigations. Unfortunately, this is not easily done since the investigation by Reed [1972] and Krynski & Schwarz [1977] solve for different quantities than those determined here and since the initial assumptions of those investigation differ considerably from those made in this work. It is tempting to compare the results of this work with those of a similar study involving satellite to satellite tracking by Hajela [1983]. For 30´x30´ areas, Hajela determined the accuracy of the predicted mean gravity anomaly to be 18.1 mgal. However, this result was for a mean gravity anomaly referred to the GEM 9 gravity field model. The results of the present report are referred to the 180 degree and order DEC 81 gravity model of Rapp. Hence, the accuracies reported in this work are expected to be better since the modeled degree variances between degrees 20 and 180, as used in Hajela's study, are replaced by the error degree variances implied by the DEC 81 coefficient variances which have considerably smaller spectral power (cf Figure 11a).

The rapid error analysis procedure of Jekeli & Rapp [1980] has been used in this report to generate Figures 1a, 1b and 7. The procedure utilizes the Tscherning & Rapp degree variance model and for the construction of the figures mentioned above, Tscherning & Rapp's degree variance parameters have been used. A portion of the results used in the construction of the figures is given in Table 5 along with results from other runs of the procedure using Jekeli's parameters

(indicated by Jek). The procedure assumes that the entire global data set of measurements is used in the computation of gravity anomaly or height anomaly accuracies. The accuracies computed by the procedure are expected to be better than those computed by the local collocation algorithm developed here. This is especially true for the height anomaly accuracy since the procedure includes, in its computation, the long wavelength spectrum which comprise the bulk of the total height anomaly signal. The best accuracies from the local collocation algorithm tested in this study are (for 30′x30′ means at gradiometer altitude of 200 km, 10^{-3} E instrument accuracy): 9.1 mgal and 43.3 cm (Figures 13f and 13g) for gravity anomalies and height anomalies respectively, where the DEC 81 coefficient errors are included. The perfect gravity field case yielded best values of 8.9 mgal and 13.6 cm. From Table 5, the corresponding accuracies computed by the rapid analysis procedure are 5.8 mgal and 9.4 cm. Therefore the differences of 3.1 mgal and 4.2 cm between the local collocation algorithm (with perfect potential coefficients) and the rapid analysis procedure is due to neglecting the region exterior to the grid in the local collocation algorithm as well as to the smoothing effects incured during the gridding of the data. The gravity anomaly accuracy can be improved by lowering the mission altitude, by increasing the instrument sensitivity, or by increasing the gridded data density. There are difficulties associated with all three ways to improve the accuracy. Lowering the altitude will increase the drag of the satellite thereby necessitating a disturbance compensation system similar to that proposed for GRM. Increasing instrument sensitivity may be possible with more research by instrument designers (some designers are optimistic that gradiometers may achieve 10^{-5} E sensitivity levels in the near future. The difficulties associated with atmospheric drag and gradiometer sensitivity are mission design considerations. The increasing of the gridded data density is more directly a data reduction problem. More specifically, when the gridded data is densified, a larger inversion process entails, thus increasing the computational demand. Two factors limit the gridded data density. One is physical, the other is economical. The physical limit is due to the

fact that the data connot be gridded more densely than the spacing of the raw gradient measurements made in the satellite orbit. To do so would introduce large errors in the high frequency spectrum of the gradients. The economic limit is one acceptable CPU-time required for the inversion. This of course, is a more subjective limit which depends on many factors. Nevertheless, it should be kept in mind during the selection of satellite gradiometer data reduction algorithm.

Table 5. 30′x30′ mean accuracies implied by Jekeli & Rapp's rapid analysis procedure. 1 sec data integration period.

Measurement Accuracy (E)	Altitude (km)	Param.	DEC 81 errors?	TOTAL RMS ERRORS Grav. Anom. (mgal)	Height Anom. (cm)
0.001	160	T/R	N	4.8	6.3
0.001	160	JEK	N	3.8	5.2
0.001	200	T/R	N	7.3	11.4
0.001	200	T/R	Y	7.5	11.7
0.001	200	JEK	N	5.8	9.4
0.0001	160	T/R	N	2.9	3.1
0.0001	160	JEK	N	2.2	2.5
0.0001	200	T/R	N	5.1	6.7
0.0001	200	JEK	N	3.9	15.4
*1.0 μ/s	160	T/R	N	8.9	15.6
*1.0 μ/s	160	JEK	N	7.1	13.0

*GRM parameters, 4s data integration, 300 km satellite separation

5.2 Conclusions and Recommendations

This report has described the data reduction of satellite born gradiometry measurements by the local collocation method. Only the error analysis aspect has been investigated in this study since no test data yet exists. The algorithm was simplified to utilize only the anomalous vertical gravity gradients gridded at altitude. The anomalous

gradients are determined by removing reference gravity gradients computed from a high degree and order geopotential model. The uncertainties of the reference geopotential coefficients must be included in the covariance computations. Two cases were considered: one, where the uncertainties of Rapp's DEC 81 geopotential model [Rapp (1981)] were included in the covariance computations, and the other, where the gravity model to degree and order 180 was considered perfect. This was done to test the sensitivity of the resulting gravimetric accuracies to the uncertainties in the reference geopotential coefficients. It was shown that the height anomaly accuracy is indeed very sensitive to the influence of reference coefficient uncertainties which follows quite naturally since the height anomaly is a low frequency phenomenon and the coefficient uncertainties will contain these low frequencies. The gravity anomaly accuracy, on the other hand, did not improve as dramatically when the coefficient errors were removed. The results of this sensitivity study indicate that the accuracies of the gravimetric quantities computed by the local collocation algorithm significantly improve with better geopotential models. More accurate geopotential models should be available in the future when the satellite gradiometer mission is attempted. These models can be easily applied to the algorithm to provide more accurate gravimetric reductions.

Further improvement may result with the inclusion of other gradient components (notably, those with at least one radial derivative). Krynski & Schwarz [1977] reported 15% to 20% accuracy improvement in the geoid undulation when the T_{13} and T_{23} components were included. This could not be confirmed in this study due to software related difficulties. A drawback caused by inclusion of the T_{13} and T_{23} components results in the increased dimension of $C_{\ell\ell}$ by a factor of three, further exacerbating the CPU time required for the matrix inversion.

The difficulties with large matrix inversion has been mentioned several times in this report. Increasing the amount of data, either by

increasing data densities or by including other gradient components, will most certainly increase the CPU time as well as possibly degrading the stability of the inversion. Although these two aspects were not studied specifically, it is possible to suggest techniques to overcome these difficulties. The technique of frequency domain collocation provides a means for handling large amounts of data by reducing the computational demands incurred by the inversion process. The early study by Tait [1983] examined this possibility for airborne gravity gradiometry with rather promising results. This concept could be extended to satellite altitudes to test the validity of the technique. To stabilize the inversion process a new technique described by Jekeli [1985] may be very useful. The technique is known as Virtual Optimal Estimation which provides a stable method to invert an ill conditioned (or "almost" ill conditioned) symmetric definite matrix through iterative techniques. With this method, error introduced by an unstable inversion process can be avoided thereby strengthening the collocation solution.

The local collocation algorithm was devised as an alternative method to compute surface mean anomalies based on data acquired by a satellite gradiometer mission. The accuracy results and ensuing discussion illustrates the behavior of the system with regard to data coverage, data density, altitude, and reference coefficient uncertainties. All of these factors play a crucial role in the accuracy of the computed mean gravity or height anomalies. To bring the mean gravity anomaly accuracies below the 5 mgal level using this algorithm, it is recommended that the mission altitude be kept as low as possible (e.g. 160 km), the data be gridded as densely as possible (e.g. $<15'$), the gradiometer designed to be as sensitive as possible (e.g. $<10^{-3}$ E), and that the gravity model to be used for the computations of the reference gradients have the smallest coefficient uncertainties as possible. More research is needed to further refine the algorithm and to fully test its effectiveness by means of a simulation.

APPENDIX A

Spherical Harmonic Expansions of the Reference Gradients

In section (III.2), it was shown that the "observed" gravity gradients in the local level coordinate system need to be centered in order to apply the least-squares collocation technique. The method to center the observations involves computing reference gravity gradients at points on the same geographical grid for which the observed gradients are known. The centered observation is then the difference of the observed gradient minus the reference gradient. In this appendix are found the expressions for the reference gradients given in terms of the reference geopotential model which are needed in equation (III.7). Reed [1973] originally derived the spherical harmonic expressions that are given here for ease of reference.

Using the local level coordinate system defined in Figure 3, the expressions are:

$$U_{11}(\Phi,\ \lambda,\ r) = \frac{GM}{r^3}\left[-1 + \sum_{n=2}^{N}\left(\frac{a}{r}\right)^n \sum_{m=0}^{n}\left(C'_{nm}\cos m\lambda + S'_{nm}\sin m\lambda\right) P_{nm}^{11}(\sin\Phi)\right] \tag{A.1}$$

$$U_{22}(\Phi,\ \lambda,\ r) = \frac{GM}{r^3}\left[-1 + \sum_{n=2}^{N}\left(\frac{a}{r}\right)^n \sum_{m=0}^{n}\left(C'_{nm}\cos m\lambda + S'_{nm}\sin m\lambda\right) P_{nm}^{22}(\sin\Phi)\right] \tag{A.2}$$

$$U_{33}(\phi, \lambda, r) = \frac{GM}{r^3}\left[\, 2 + \sum_{n=2}^{N}\left(\frac{a}{r}\right)^n \sum_{m=0}^{n} (C'_{nm}\cos m\lambda + S'_{nm}\sin m\lambda)\, P^{33}_{nm}(\sin\phi)\right] \tag{A.3}$$

$$U_{12}(\phi, \lambda, r) = \frac{GM}{r^3}\sum_{n=2}^{N}\left(\frac{a}{r}\right)^n \sum_{m=0}^{n} (C'_{nm}\cos m\lambda - S'_{nm}\sin m\lambda)\, P^{12}_{nm}(\sin\phi)\Big] \tag{A.4}$$

$$U_{13}(\phi, \lambda, r) = \frac{GM}{r^3}\sum_{n=2}^{N}\left(\frac{a}{r}\right)^n \sum_{m=0}^{n} (C'_{nm}\cos m\lambda - S'_{nm}\sin m\lambda)\, P^{13}_{nm}(\sin\phi)\Big] \tag{A.5}$$

$$U_{23}(\phi, \lambda, r) = \frac{GM}{r^3}\sum_{n=2}^{N}\left(\frac{a}{r}\right)^n \sum_{m=0}^{n} (C'_{nm}\cos m\lambda + S'_{nm}\sin m\lambda)\, P^{23}_{nm}(\sin\phi)\Big] \tag{A.6}$$

where the N denotes the maximum degree of the reference geopotential model. The observed gradients can be expressed by allowing N to approach infinity and by substituting the unnormalized (conventional) geopotential coefficients C_{nm}, S_{nm} for the conventional reference geopotential coefficients C'_{nm}, S'_{nm}. The superscripts attached to the conventional associated Legendre functions denote the differentiations. Reed [1973] also provides these differentiated functions in terms of non-differentiated Legendre functions:

$$P^{11}_{nm}(\sin\phi) = \left[\frac{m\sin^2\phi - m^2}{\cos^2\phi} - (n+1)\right]P_{nm}(\sin\phi) - \tan\phi\, P_{n,m+1}(\sin\phi) \tag{A.7}$$

$$P^{22}_{nm}(\sin\phi) = \left[\frac{m^2 - m\sin^2\phi}{\cos^2\phi} - (n+1)^2\right]P_{nm}(\sin\phi) + \tan\phi\, P_{n,m+1}(\sin\phi) \tag{A.8}$$

$$P^{33}_{nm}(\sin\phi) = (n+1)(n+2)P_{nm}(\sin\phi) \tag{A.9}$$

$$P^{12}_{nm}(\sin\bar{\phi}) = -\frac{m(m-1)\sin\bar{\phi}}{\cos^2\bar{\phi}} P_{nm}(\sin\bar{\phi}) + \frac{m}{\cos\bar{\phi}} P_{n,m+1}(\sin\bar{\phi}) \qquad (A.10)$$

$$P^{13}_{nm}(\sin\bar{\phi}) = -\frac{m(n+2)}{\cos\bar{\phi}} P_{nm}(\sin\bar{\phi}) \qquad (A.11)$$

$$P^{23}_{nm}(\sin\bar{\phi}) = m(n+2)\tan\bar{\phi}\, P_{nm}(\sin\bar{\phi}) - (n+2)\, P_{n,m+1}(\sin\bar{\phi}) \qquad (A.12)$$

The $P_{nm}(\sin\bar{\phi})$ and $P_{n,m+1}(\sin\bar{\phi})$ terms can be found from familiar recursion formulas such as (Ilk [1983]);

$$(n-m)P_{nm}(t) = (2n-1)tP_{n-1,m}(t) - (n+m-1)P_{n-2,m}(t) \qquad (A.13)$$

$$(1-t^2)^{\frac{1}{2}}P_{nm}(t) = (2m-1)tP_{n,m-1}(t) - (n+m-1)(n-m+2)(1-t^2)^{\frac{1}{2}}P_{n,m-2}(t) \qquad (A.14)$$

APPENDIX B

Gradient Covariance Expressions

In this appendix, the explicit covariance expressions are given for reference. The expressions are nothing more than applications of the covariance propagation law (Moritz, [1980])

$$C_{ij}(P,Q) = L_i^P L_j^Q K(P,Q) \qquad (B.1)$$

from which all gravimetric covariances can be related to the disturbing potential covariance K(P,Q) by the functional L_i and L_j applied at the point P and Q. The covariance function of the disturbing potential is only a function of the relative location of the points P and Q. On the sphere, this can be written as (Moritz, [1980])

$$K(P,Q) = K(r_P, r_Q, \psi_{PQ}) = K \qquad (B.2)$$

where r_P and r_Q are the geocentric radial distances of the points P and Q and ψ_{PQ} is the spherical distance of P and Q given in terms of their respective co-latitude and longitude as ($\theta = \pi/2 - \tilde{\phi}$),

$$\cos\psi_{PQ} = \cos\theta_P\cos\theta_Q + \sin\theta_P\sin\theta_Q\cos(\lambda_Q-\lambda_P) \qquad (B.3)$$

Thus the covariance of the disturbing potential is isotropic and stationary.

Using the functionals given in equations (III.15) to (III.18), the covariances are determined and presented for reference below. Those functionals with a prime attached denote that the functional is to be applied at the point Q. Unprimed quantities refer to P.

I. Autocovariances of the observation covariance matrix, C_{tt}

$$\mathrm{Cov}[T_{11}(P),T_{11}(Q)] = \left[\frac{1}{r^2\cos^2\bar{\phi}}\frac{\partial^2}{\partial\lambda^2} - \frac{\tan\bar{\phi}}{r^2}\frac{\partial}{\partial\bar{\phi}} + \frac{1}{r}\frac{\partial}{\partial r}\right]^1 \cdot$$

$$\left[\frac{1}{r'^2\cos^2\bar{\phi}'}\frac{\partial^2 K}{\partial\lambda'^2} - \frac{\tan\bar{\phi}'}{r'^2}\frac{\partial K}{\partial\bar{\phi}'} + \frac{1}{r'}\frac{\partial K}{\partial r'}\right] =$$

$$= \frac{1}{r^2r'^2\cos^2\bar{\phi}\cos^2\bar{\phi}'}\frac{\partial^4 K}{\partial\lambda^2\partial\lambda'^2} - \frac{\tan\bar{\phi}'}{r^2r'^2\cos^2\bar{\phi}}\frac{\partial^3 K}{\partial\lambda^2\partial\bar{\phi}'} + \frac{1}{r^2r'\cos^2\bar{\phi}}\frac{\partial^3 K}{\partial^2\lambda\partial r'}$$

$$- \frac{\tan\bar{\phi}}{r^2r'^2\cos^2\bar{\phi}'}\frac{\partial^3 K}{\partial\bar{\phi}\partial\lambda'^2} + \frac{\tan\bar{\phi}\tan\bar{\phi}'}{r^2r'^2}\frac{\partial^2 K}{\partial\bar{\phi}\partial\bar{\phi}'} - \frac{\tan\bar{\phi}}{r^2r'}\frac{\partial^2 K}{\partial\bar{\phi}\partial r'}$$

$$+ \frac{1}{rr'^2\cos^2\bar{\phi}'}\frac{\partial^3 K}{\partial r\partial\lambda'^2} - \frac{\tan\bar{\phi}'}{rr'^2}\frac{\partial^2 K}{\partial r\partial\bar{\phi}'} + \frac{1}{rr'}\frac{\partial^2 K}{\partial r\partial r'} \qquad \text{(B.4)}$$

$$\mathrm{Cov}[T_{22}(P),T_{22}(Q)] = \left[\frac{1}{r^2}\frac{\partial^2}{\partial\bar{\phi}^2} + \frac{1}{r}\frac{\partial}{\partial r}\right]\left[\frac{1}{r'^2}\frac{\partial^2 K}{\partial\bar{\phi}'^2} + \frac{1}{r'}\frac{\partial K}{\partial r'}\right]$$

$$= \frac{1}{r^2r'^2}\frac{\partial^4 K}{\partial\bar{\phi}^2\partial\bar{\phi}'^2} + \frac{1}{r^2r'}\frac{\partial^3 K}{\partial\bar{\phi}^2\partial r'} + \frac{1}{rr'^2}\frac{\partial^3 K}{\partial r\partial\bar{\phi}'^2} + \frac{1}{rr'}\frac{\partial^2 K}{\partial r\partial r'} \qquad \text{(B.5)}$$

$$\mathrm{Cov}[T_{33}(P),T_{33}(Q)] = \frac{\partial^4 K}{\partial r^2\partial_{r'^2}} \qquad \text{(B.6)}$$

$$\mathrm{Cov}[T_{12}(P),T_{12}(Q)] = \left[\frac{1}{r^2\cos\bar{\phi}}\frac{\partial^2}{\partial\lambda\partial\bar{\phi}} + \frac{\tan\bar{\phi}}{r^2}\frac{\partial}{\partial\lambda}\right]\left[\frac{1}{r'^2\cos\bar{\phi}'}\frac{\partial^2 K}{\partial\lambda\partial\bar{\phi}'} + \frac{\tan\bar{\phi}'}{r'^2}\frac{\partial K}{\partial\lambda'}\right]$$

$$= \frac{1}{r^2r'^2\cos\bar{\phi}\cos\bar{\phi}'}\frac{\partial^4 K}{\partial\lambda\partial\bar{\phi}\partial\lambda'\partial\bar{\phi}'} + \frac{\tan\bar{\phi}'}{r^2r'^2\cos\bar{\phi}}\frac{\partial^3 K}{\partial\lambda\partial\bar{\phi}\partial\lambda'}$$

$$+ \frac{\tan\bar{\phi}}{r^2r'^2\cos\bar{\phi}'}\frac{\partial^3 K}{\partial\lambda\partial\lambda'\partial\bar{\phi}'} + \frac{\tan\bar{\phi}\tan\bar{\phi}'}{r^2r'^2}\frac{\partial^2 K}{\partial\lambda\partial\lambda'} \qquad \text{(B.7)}$$

$$\mathrm{Cov}[T_{13}(P),T_{13}(Q)] = \left[\frac{1}{r\cos\bar{\phi}}\frac{\partial^2}{\partial\lambda\partial r} - \frac{1}{r^2\cos\bar{\phi}}\frac{\partial}{\partial\lambda}\right]$$

$$\left[\frac{1}{r'\cos\bar{\phi}'}\frac{\partial^2 K}{\partial\lambda'\partial r'} - \frac{1}{r'^2\cos\bar{\phi}'}\frac{\partial K}{\partial\lambda}\right]$$

$$= \frac{1}{rr'\cos\bar{\phi}\cos\bar{\phi}'}\frac{\partial^4 K}{\partial\lambda\partial r\partial\lambda'\partial r'} - \frac{1}{rr'^2\cos\bar{\phi}\cos\bar{\phi}'}\frac{\partial^3 K}{\partial\lambda\partial r\partial\lambda'}$$

$$- \frac{1}{r^2r'\cos\bar{\phi}\cos\bar{\phi}'}\frac{\partial^3 K}{\partial\lambda'\partial r'\partial\lambda} + \frac{1}{r^2r'^2\cos\bar{\phi}\cos\bar{\phi}'}\frac{\partial^2 K}{\partial\lambda\partial\lambda'} \qquad \text{(B.8)}$$

$$\mathrm{Cov}[T_{23}(P),T_{23}(Q)] = \left[\frac{1}{r}\frac{\partial^2}{\partial\bar{\phi}\partial r} - \frac{1}{r^2}\frac{\partial}{\partial\bar{\phi}}\right]\left[\frac{1}{r'}\frac{\partial^2 K}{\partial\bar{\phi}'\partial r'} - \frac{1}{r'^2}\frac{\partial K}{\partial\bar{\phi}'}\right]$$

$$= \frac{1}{rr'}\frac{\partial^4 K}{\partial\bar{\phi}\partial r\partial\bar{\phi}'\partial r'} - \frac{1}{rr'^2}\frac{\partial^3 K}{\partial\bar{\phi}\partial r\partial\bar{\phi}'} - \frac{1}{r^2r'}\frac{\partial^3 K}{\partial\bar{\phi}\partial\bar{\phi}'\partial r'} + \frac{1}{r^2r'^2}\frac{\partial^2 K}{\partial\bar{\phi}\partial\bar{\phi}'} \qquad \text{(B.9)}$$

II. Cross covariances of the observation covariance matrix, C_{tt}.

$$\mathrm{Cov}[T_{11}(P),T_{22}(Q)] = \frac{1}{r^2r'^2\cos^2\bar{\phi}}\frac{\partial^4 K}{\partial\lambda^2\partial\bar{\phi}'^2} + \frac{1}{r^2r'\cos^2\bar{\phi}}\frac{\partial^3 K}{\partial\lambda^2\partial r'}$$

$$- \frac{\tan\bar{\phi}}{r^2r'^2}\frac{\partial^3 K}{\partial\bar{\phi}\partial\bar{\phi}'^2} - \frac{\tan\bar{\phi}}{r^2r'}\frac{\partial^2 K}{\partial\bar{\phi}\partial r'} + \frac{1}{rr'^2}\frac{\partial^3 K}{\partial r\partial\bar{\phi}'^2} + \frac{1}{rr'}\frac{\partial^2 K}{\partial r\partial r'} \qquad \text{(B.10)}$$

$$\mathrm{Cov}[T_{11}(P),T_{33}(Q)] = \frac{1}{r^2\cos^2\bar{\phi}}\frac{\partial^4 K}{\partial\lambda^2\partial r'^2} - \frac{\tan\bar{\phi}}{r^2}\frac{\partial^3 K}{\partial\bar{\phi}\partial r'^2} + \frac{1}{r}\frac{\partial^3 K}{\partial r\partial r'^2} \qquad \text{(B.11)}$$

$$\mathrm{Cov}[T_{11}(P),T_{12}(Q)] = \frac{1}{r^2r'^2\cos^2\bar{\phi}\cos\bar{\phi}'}\frac{\partial^4K}{\partial\lambda^2\partial\lambda'\partial\bar{\phi}'} + \frac{\tan\bar{\phi}'}{r^2r'^2\cos^2\bar{\phi}}\frac{\partial^3K}{\partial\lambda^2\partial\lambda'}$$

$$- \frac{\tan\bar{\phi}}{r^2r'^2\cos\bar{\phi}'}\frac{\partial^3K}{\partial\bar{\phi}\partial\lambda'\partial\bar{\phi}'} - \frac{\tan\bar{\phi}\tan\bar{\phi}'}{r^2r'^2}\frac{\partial^2K}{\partial\bar{\phi}\partial\lambda'} + \frac{1}{rr'^2\cos\bar{\phi}'}\frac{\partial^3K}{\partial r\partial\lambda'\partial\bar{\phi}'}$$

$$+ \frac{\tan\bar{\phi}'}{rr'^2}\frac{\partial^2K}{\partial r\partial\lambda'} \qquad \text{(B.12)}$$

$$\mathrm{Cov}[T_{11}(P),T_{13}(Q)] = \frac{1}{r^2r'\cos^2\bar{\phi}\cos\bar{\phi}'}\frac{\partial^4K}{\partial\lambda^2\partial\lambda'\partial r'} - \frac{1}{r^2r'^2\cos^2\bar{\phi}\cos\bar{\phi}'}\frac{\partial^3K}{\partial\lambda^2\partial\lambda'}$$

$$- \frac{\tan\bar{\phi}}{r^2r'\cos\bar{\phi}'}\frac{\partial^3K}{\partial\bar{\phi}\partial\lambda'\partial\bar{\phi}'} + \frac{\tan\bar{\phi}}{r^2r'^2\cos\bar{\phi}'}\frac{\partial^2K}{\partial\bar{\phi}\partial\lambda'} + \frac{1}{rr'\cos\bar{\phi}'}\frac{\partial^3K}{\partial r\partial\lambda'\partial r'}$$

$$- \frac{1}{rr'^2\cos\bar{\phi}'}\frac{\partial^2K}{\partial r\partial\lambda'} \qquad \text{(B.13)}$$

$$\mathrm{Cov}[T_{11}(P),T_{23}(Q)] = \frac{1}{r^2r'\cos^2\bar{\phi}}\frac{\partial^4K}{\partial\lambda^2\partial\bar{\phi}'\partial r'} - \frac{1}{r^2r'^2\cos^2\bar{\phi}}\frac{\partial^3K}{\partial\lambda^2\partial\bar{\phi}'}$$

$$- \frac{\tan\bar{\phi}}{r^2r'}\frac{\partial^3K}{\partial\bar{\phi}\partial\bar{\phi}'\partial r'} + \frac{\tan\bar{\phi}}{r^2r'^2}\frac{\partial^2K}{\partial\bar{\phi}\partial\bar{\phi}'} + \frac{1}{rr'}\frac{\partial^3K}{\partial r\partial\bar{\phi}'\partial r'} - \frac{1}{rr'^2}\frac{\partial^2K}{\partial r\partial\bar{\phi}'} \qquad \text{(B.14)}$$

$$\mathrm{Cov}[T_{22}(P),T_{33}(Q)] = \frac{1}{r^2}\frac{\partial^2K}{\partial\bar{\phi}^2\partial r'^2} + \frac{1}{r}\frac{\partial^3K}{\partial r\partial r'^2} \qquad \text{(B.15)}$$

$$\mathrm{Cov}[T_{22}(P),T_{12}(Q)] = \frac{1}{r^2r'^2\cos\bar{\phi}'}\frac{\partial^4K}{\partial\bar{\phi}^2\partial\lambda'\partial\bar{\phi}'} + \frac{\tan\bar{\phi}'}{r^2r'^2}\frac{\partial^3K}{\partial\bar{\phi}^2\partial\lambda'}$$

$$+ \frac{1}{rr'^2\cos\bar{\phi}'}\frac{\partial^3K}{\partial r\partial\lambda'\partial\bar{\phi}'} + \frac{\tan\bar{\phi}'}{rr'^2}\frac{\partial^2K}{\partial r\partial\lambda'} \qquad \text{(B.16)}$$

$$\mathrm{Cov}[T_{22}(P),T_{13}(Q)] = \frac{1}{r^2r'\cos\bar{\phi}'}\frac{\partial^4K}{\partial\bar{\phi}^2\partial\lambda'\partial r'} - \frac{1}{r^2r'^2\cos\bar{\phi}'}\frac{\partial^3K}{\partial\bar{\phi}^2\partial\lambda'}$$

$$+ \frac{1}{rr'\cos\bar{\phi}'}\frac{\partial^3K}{\partial r\partial\lambda'\partial r'} - \frac{1}{rr'^2\cos\bar{\phi}}\frac{\partial^2K}{\partial r\partial\lambda'} \qquad \text{(B.17)}$$

$$\mathrm{Cov}[T_{22}(P),T_{23}(Q)] = \frac{1}{r^2r'}\frac{\partial^4K}{\partial\bar{\phi}^2\partial\bar{\phi}'\partial r'} - \frac{1}{r^2r'^2}\frac{\partial^3K}{\partial\bar{\phi}^2\partial\bar{\phi}'} + \frac{1}{rr'}\frac{\partial^3K}{\partial r\partial\bar{\phi}'\partial r'}$$

$$- \frac{1}{rr'^2}\frac{\partial^2K}{\partial r\partial\bar{\phi}'} \qquad \text{(B.18)}$$

$$\mathrm{Cov}[T_{33}(P),T_{12}(Q)] = \frac{1}{r'^2\cos\bar{\phi}'}\frac{\partial^4K}{\partial r^2\partial\lambda'\partial\bar{\phi}'} + \frac{\tan\bar{\phi}'}{r'^2}\frac{\partial^3K}{\partial r^2\partial\lambda'} \qquad \text{(B.19)}$$

$$\mathrm{Cov}[T_{33}(P),T_{13}(Q)] = \frac{1}{r'\cos\bar{\phi}'}\frac{\partial^4K}{\partial r^2\partial\lambda'\partial r'} - \frac{1}{r'^2\cos\bar{\phi}'}\frac{\partial^3K}{\partial r^2\partial\lambda'} \qquad \text{(B.20)}$$

$$\mathrm{Cov}[T_{33}(P),T_{23}(Q)] = \frac{1}{r'}\frac{\partial^4K}{\partial r^2\partial\bar{\phi}'\partial r'} - \frac{1}{r'^2}\frac{\partial^3K}{\partial r^2\partial\bar{\phi}'} \qquad \text{(B.21)}$$

$$\mathrm{Cov}[T_{12}(P),T_{13}(Q)] = \frac{1}{r^2r'\cos\bar{\phi}\cos\bar{\phi}'}\frac{\partial^4K}{\partial\lambda\partial\bar{\phi}\partial\lambda'\partial r'} - \frac{1}{r^2r'^2\cos\bar{\phi}\cos\bar{\phi}'}\frac{\partial^3K}{\partial\lambda\partial\bar{\phi}\partial\lambda'}$$

$$+ \frac{\tan\bar{\phi}}{r^2r'\cos\bar{\phi}'}\frac{\partial^3K}{\partial\lambda\partial\lambda'\partial r'} - \frac{\tan\bar{\phi}}{r^2r'^2\cos\bar{\phi}'}\frac{\partial^2K}{\partial\lambda\partial\lambda'} \qquad \text{(B.22)}$$

$$\mathrm{Cov}[T_{12}(P),T_{23}(Q)] = \frac{1}{r^2r'\cos\bar{\phi}}\frac{\partial^4K}{\partial\lambda\partial\bar{\phi}\partial\bar{\phi}'\partial r'} - \frac{1}{r^2r'^2\cos\bar{\phi}}\frac{\partial^3K}{\partial\lambda\partial\bar{\phi}\partial\bar{\phi}'}$$

$$+ \frac{\tan\bar{\phi}}{r^2r'}\frac{\partial^3K}{\partial\lambda\partial\bar{\phi}'\partial r'} - \frac{\tan\bar{\phi}}{r^2r'^2}\frac{\partial^2K}{\partial\lambda\partial\bar{\phi}'} \qquad \text{(B.23)}$$

$$\mathrm{Cov}[T_{13}(P),T_{23}(Q)] = \frac{1}{rr'\cos\bar{\phi}}\frac{\partial^4K}{\partial\lambda\partial r\partial\bar{\phi}'\partial r'} - \frac{1}{rr'^2\cos\bar{\phi}}\frac{\partial^3K}{\partial\lambda\partial r\partial\bar{\phi}'}$$

$$- \frac{1}{r^2r'\cos\bar{\phi}}\frac{\partial^3K}{\partial\lambda\partial\bar{\phi}'\partial r'} + \frac{1}{r^2r'^2\cos\bar{\phi}}\frac{\partial^2K}{\partial\lambda\partial\bar{\phi}'} \qquad \text{(B.24)}$$

III. Cross covariance matrix, C_{gt}

a. Gravity anomalies, Δg.

$$\mathrm{Cov}[\Delta g(P),T_{11}(Q)] = -\frac{1}{r'^2\cos^2\bar{\phi}'}\frac{\partial^3 K}{\partial r\partial\lambda'^2} + \frac{\tan\bar{\phi}'}{r'^2}\frac{\partial^2 K}{\partial r\partial\bar{\phi}'} - \frac{1}{r'}\frac{\partial^2 K}{\partial r\partial r'}$$

$$-\frac{2}{rr'^2\cos^2\bar{\phi}'}\frac{\partial^2 K}{\partial\lambda'^2} + \frac{2\tan\bar{\phi}'}{rr'^2}\frac{\partial K}{\partial\bar{\phi}'} - \frac{2}{rr'}\frac{\partial K}{\partial r'} \qquad \text{(B.25)}$$

$$\mathrm{Cov}[\Delta g(P),T_{22}(Q)] = -\frac{1}{r'^2}\frac{\partial^3 K}{\partial r\partial\bar{\phi}'^2} - \frac{1}{r'}\frac{\partial^2 K}{\partial r\partial r'} - \frac{2}{rr'^2}\frac{\partial^2 K}{\partial\bar{\phi}'^2} - \frac{2}{rr'}\frac{\partial K}{\partial r'}$$

(B.26)

$$\mathrm{Cov}[\Delta g(P),T_{33}(Q)] = -\frac{\partial^3 K}{\partial r\partial r'^2} - \frac{2}{r}\frac{\partial^2 K}{\partial r'^2} \qquad \text{(B.27)}$$

$$\mathrm{Cov}[\Delta g(P),T_{12}(Q)] = -\frac{1}{r'^2\cos\bar{\phi}'}\frac{\partial^3 K}{\partial r\partial\lambda'\partial\bar{\phi}'} - \frac{\tan\bar{\phi}}{r^2}\frac{\partial^2 K}{\partial r\partial\lambda'} - \frac{2}{rr'^2\cos\bar{\phi}'}\frac{\partial^2 K}{\partial\lambda'\partial\bar{\phi}'}$$

$$-\frac{2}{rr'^2\cos\bar{\phi}'}\frac{\partial K}{\partial\lambda'} \qquad \text{(B.28)}$$

$$\mathrm{Cov}[\Delta g(P),T_{13}(Q)] = -\frac{1}{r'\cos\bar{\phi}'}\frac{\partial^3 K}{\partial r\partial\lambda'\partial r'} + \frac{1}{r'^2\cos\bar{\phi}'}\frac{\partial^2 K}{\partial r\partial\lambda} - \frac{2}{rr'\cos\bar{\phi}'}\frac{\partial^2 K}{\partial\lambda'\partial r'}$$

$$+\frac{2}{rr'^2\cos\bar{\phi}'}\frac{\partial K}{\partial\lambda} \qquad \text{(B.29)}$$

$$\mathrm{Cov}[\Delta g(P),T_{23}(Q)] = -\frac{1}{r'}\frac{\partial^3 K}{\partial r\partial\bar{\phi}'\partial r'} - \frac{1}{r'^2}\frac{\partial^2 K}{\partial r\partial\bar{\phi}'} - \frac{2}{rr'}\frac{\partial^2 K}{\partial\bar{\phi}'\partial r'} - \frac{2}{rr'^2}\frac{\partial K}{\partial\bar{\phi}'}$$

(B.30)

B. Height anomaly ζ ($\approx$ N the geoid height).

$$\mathrm{Cov}[\zeta(P),T_{11}(Q)] = \frac{1}{\gamma_0}\left[\frac{1}{r'^2\cos^2\bar{\phi}'}\frac{\partial^2 K}{\partial\lambda'^2} - \frac{\tan\bar{\phi}'}{r'^2}\frac{\partial K}{\partial\bar{\phi}'} + \frac{1}{r'}\frac{\partial K}{\partial r'}\right] \qquad (B.31)$$

$$\mathrm{Cov}[\zeta(P),T_{22}(Q)] = \frac{1}{\gamma_0}\left[\frac{1}{r'^2}\frac{\partial^2 K}{\partial\bar{\phi}'^2} + \frac{1}{r'}\frac{\partial K}{\partial r'}\right] \qquad (B.32)$$

$$\mathrm{Cov}[\zeta(P),T_{33}(Q)] = \frac{1}{\gamma_0}\frac{\partial^2 K}{\partial r'^2} \qquad (B.33)$$

$$\mathrm{Cov}[\zeta(P),T_{12}(Q)] = \frac{1}{\gamma_0}\left[\frac{1}{r'^2\cos\bar{\phi}'}\frac{\partial^2 K}{\partial\lambda'\partial\bar{\phi}'} + \frac{\tan\bar{\phi}'}{r'^2}\frac{\partial K}{\partial\lambda'}\right] \qquad (B.34)$$

$$\mathrm{Cov}[\zeta(P),T_{13}(Q)] = \frac{1}{\gamma_0}\left[\frac{1}{r'\cos\bar{\phi}'}\frac{\partial^2 K}{\partial\lambda'\partial r'} - \frac{1}{r'^2\cos\bar{\phi}}\frac{\partial K}{\partial\lambda'}\right] \qquad (B.35)$$

$$\mathrm{Cov}[\zeta(P),T_{23}(Q)] = \frac{1}{\gamma_0}\left[\frac{1}{r'}\frac{\partial K}{\partial\bar{\phi}\partial r'} - \frac{1}{r'^2}\frac{\partial K}{\partial\bar{\phi}'}\right] \qquad (B.36)$$

IV. The auto covariances of the predicted signals, C_{ss}.

From Moritz [1980], page 108,

$$\mathrm{Cov}[\Delta g(P),\Delta g(Q)] = \frac{\partial^2 K}{\partial r\partial r'} + \frac{2}{r'}\frac{\partial K}{\partial r} + \frac{2}{r}\frac{\partial K}{\partial r'} + \frac{4}{rr'}K \qquad (B.37)$$

and for the height anomaly,

$$\mathrm{Cov}[\zeta(P),\zeta(Q)] = \frac{1}{\gamma_0^2}K. \qquad (B.38)$$

Appendix C. Listing of program GIFRAD

```
C
C
C    PROGRAM GIFRAD: A PROGRAM WHICH COMPUTES THE EXPECTED ERROR
C                    IN A MEAN GRAVITY OR HEIGHT ANOMALY BASED
C                    UPON RADIAL/RADIAL GRADIOMETERY MEASUREMENTS
C                    OVER A GRID OF FIXED SIZE.
C
C    WRITTEN BY: JOHN W. ROBBINS
C    DATE: FEBRUARY 1, 1985
C    VERS: FEBRUARY 17, 1985
C    RUN : FEBRUARY 20, 1985
C
C    DEPARTMENT OF GEODETIC SCIENCE AND SURVEYING
C    OHIO STATE UNIVERSITY.
C
C
      IMPLICIT REAL *8(A-H,O-Z), LOGICAL (L)
      COMMON /INTERP/COV(3,519)
      DIMENSION CXX(225,225),DIST(225,225),CSX(2,225)
      DIMENSION DSX(225),SCR(225),CSX1(1,225),CSX2(1,225)
      DIMENSION CC1(225,1),CC2(225,1),ANS(1),ANT(1)
      DIMENSION CXXI(225,225)
C     DATA CSS1,CSS2/0.11413538300,224.7384996D0/
      DATA CSS1,CSS2/1.1613600,3.0212684D2/
      DATA CLAT/40.D0/
C
C     READ IN THE COVARIANCES.
C
C     FIRST, THE CXX & CSX REQUIRED COVARIANCES ARE READ.
C
      READ(5,*)(COV(1,I),COV(2,I),COV(3,I),I=1,519)
C
C
C     END OF CXX & CSX REQUIRED COVARIANCES
C
C
C
C     WRITE THE HEADING FOR THE OUTPUT TABLE.
C
C
      WRITE(6,106)
106   FORMAT(2X,'GRID',6X,'GRID',4X,'MEAN GRAVITY',2X,'MEAN HGT.',3X,
     *'INVERS.',6X,'CSX*CXXI*CXS VALUES',/
     *2X,'WIDTH',3X,'SPACING',5X,'ANOMALY',6X,'ANOMALY',4X,'STABIL.',/
     *2X,'(DEG)',4X,'(DEG)',6X,'(MGAL)',7X,'(METERS)',12X,'(METERS**2)',
     *8X,'(MGAL**2)',//)
C
C     READ IN THE OVERALL SIZE OF THE GRID AND WHETHER OR NOT IT
C     IS THE LAST GRID SIZE TO BE CONSIDERED (LOGICAL VARIABLE: L).
C
3     READ(5,99)D,DELD,L
99    FORMAT(2F10.7,L2)
C     WRITE(6,98)D,DELD,L
C8    FORMAT(//1X,2F10.7,3X,L2)
      DDEG=D
      DDEL=DELD
      NP=IDNINT(D/DELD)+1
      NPS=NP*NP
      NPX1=(NPS+1)/2
```

```
      NPX2=NPX1+1
C
C     INITIALIZE ALL ARRAYS TO ZERO TO AVOID CARRY-OVER FROM
C     PREVIOUS COMPUTATIONS.
C
      ANS(1)=0.D0
      ANT(1)=0.D0
      DO 12 I=1,225
      DO 12 J=1,225
      DIST(I,J)=0.D0
      CXXI(I,J)=0.D0
12    CXX(I,J)=0.D0
      DO 14 I=1,2
      DO 14 J=1,225
14    CSX(I,J)=0.D0
      DO 13 I=1,225
      CSX1(1,I)=0.D0
      CSX2(1,I)=0.D0
      CC1(I,1)=0.D0
      CC2(I,1)=0.D0
13    DSX(I)=0.D0
C
C     COMPUTE THE MATRIX OF SPHERICAL DISTANCES FOR THE GRID
C     SPECIFIED FOR THE OVERALL GRID SIZE (D) AT THE LATITUDE
C     (CLAT). THE SUBROUTINE ONLY WORKS WITH RECTANGULAR GRIDS.
C     RADIALLY SYMMETRIC GRIDS MUST BE DEALT WITH DIFFERENTLY.
C
      CALL SDIS(CLAT,D,NP,NPS,DIST)
C
C     SET-UP THE COVARIANCE MATRIX, CXX.
C
      DO 11 I=1,NPS
      DO 11 J=I,NPS
11    CXX(I,J)=COVINT(DIST(I,J),1)
      DO 23 I=1,NPS
      DO 23 J=I,NPS
23    CXX(J,I)=CXX(I,J)
C
C     ADDITION OF INSTRUMENT NOISE TO DIAGONAL ELEMENTS.
C
C     THE VALUE 1.D-6 IS THE SQUARE OF THE INSTRUMENT SENSITIVITY
C     OF 1.D-3 EOTVOS UNITS.
C
C     ONE MUST REPLACE THIS VALUE FOR OTHER SENSITIVITIES.
C
      DO 24 I=1,NPS
24    CXX(I,I)=CXX(I,I)+1.D-6
C
C     SET-UP OF CSX RELATED DISTANCES.
C
      DO 21 I=1,NPX1
21    DSX(I)=DIST(I,NPX1)
      DO 22 I=NPX2,NPS
22    DSX(I)=DIST(NPX1,I)
C
C
C     SET-UP THE CSX-MATRIX.
C
      DO 31 J=1,NPS
      CSX(1,J)=COVINT(DSX(J),2)
```

```
 31     CSX(2,J)=COVINT(DSX(J),3)
        DO 33 J=1,NPS
        CSX1(1,J)=CSX(1,J)
 33     CSX2(1,J)=CSX(2,J)
C
C       MAKE COMPUTATIONS FOR THE EXPECTED ERRORS RESULTING FROM
C       THE GIVEN PARAMETERS.
C
C
C       THE SUBROUTINES LINV1F,VMULFP,VMULFF ARE PROVIDED BY
C       IMSL SUBROUTINE LIBRARY.
C
C       LINV1F: MATRIX INVERSION
C       VMULFP, VMULFF: MATRIX ALGEBRAIC OPERATIONS.
C
        CALL LINV1F(CXX,NPS,225,CXXI,5,SCR,IER)
        CALL VMULFP(CXXI,CSX1,NPS,NPS,1,225,1,CC1,225,IER1)
        CALL VMULFP(CXXI,CSX2,NPS,NPS,1,225,1,CC2,225,IER2)
        CALL VMULFF(CSX1,CC1,1,NPS,1,1,225,ANS,1,IER3)
        CALL VMULFF(CSX2,CC2,1,NPS,1,1,225,ANT,1,IER4)
        EHA=CSS1-ANS(1)
        EGA=CSS2-ANT(1)
        FGA=DSQRT(EGA)
        FHA=DSQRT(EHA)
C
C       WRITE RESULTS.
C
        WRITE(6,108)DDEG,DDEL,FGA,FHA,IER,ANS(1),ANT(1)
 108    FORMAT(F8.5,3X,F7.5,3X,F10.5,3X,F9.5,4X,I4,3X,D14.7,3X,D14.7)
        IF(.NOT.L)GO TO 3
        STOP
        END
        SUBROUTINE SDIS(CLAT,D,NP,NPS,DIST)
C
C
C*************************************************************
C
C    SUBROUTINE NOTES:  VARIABLE LIST.
C
C    1. INPUT VARIABLES IN THE CALL STATEMENT:
C
C         CLAT  :  THE LATITUDE OF THE CENTRAL POINT OF THE GRID.
C
C         D     :  THE OVERALL SIZE OF THE GRID.
C
C         NP    :  THE NUMBER OF INCREMENTS ALONG A GRID SIDE.
C
C         NPS   :  THE TOTAL NUMBER OF POINTS WITHIN THE GRID.
C
C    2. OUTPUT VARIABLE RETURNED TO MAIN PROGRAM:
C
C         DIST  :  THE ARRAY OF SPHERICAL DISTANCES IN RADIANS.
C                  IT IS UPPER-TRIANGULAR FORM.
C
C    3. VARIABLES USED WITHIN THE SUBROUTINE:
C
C         NPM1  :  NP - 1
C
C         DNP   :  1./NPM1 = 1./(NP-1), THIS GIVES THE RELATIVE
C                  GRID SPACING VALUE.
```

```
C
C         NP2    :  NP*NPM1+1 = NP**2 - NP + 1
C
C         NPMA   :  NPS - 1, TOTAL NO. OF POINTS MINUS 1.
C
C*************************************************************
C
C
      IMPLICIT REAL *8(A-H,O-Z)
      DIMENSION DIST(225,225),PLAT(225),PLON(225)
      SD(W,X,Y,Z)=DACOS(DSIN(W)*DSIN(Y)+DCOS(W)*DCOS(Y)*DCOS(Z-X))
      PI=4.DO*DATAN(1.DO)
      D=D*PI/180.DO
      BLAT=CLAT*PI/180.DO
      NPM1=NP-1
      DNP=1.DO/NPM1
      NP2=NP*NPM1+1
      NPMA=NPS-1
C
C     ESTABLISH LATITUDES AND LONGITUDES FOR EACH OF THE POINTS.
C
      DO 5 J=1,NP2,NP
      JA=J-1
      DJNP=FLOAT(JA)/FLOAT(NP)
      DO 5 I=1,NP
5     PLAT(I+JA)=BLAT+D/2.DO-DJNP*DNP*D
      DO 6 I=1,NP
      IA=I-1
      DO 6 J=1,NP2,NP
      JA=J-1
6     PLON(I+JA)=FLOAT(IA)*DNP*D
C
C     COMPUTE THE SPHERICAL DISTANCES.
C
      DO 11 I=1,NPMA
      II=I+1
      DO 11 J=II,NPS
11    DIST(I,J)=SD(PLAT(I),PLON(I),PLAT(J),PLON(J))
      DO 12 I=1,NPS
12    DIST(I,I)=0.DO
      RETURN
      END
      FUNCTION COVINT(D,ID)
C
C     FUNCTION COVINT: INTERPOLATES THE COVARIANCES REQUIRED IN
C       THE SOLUTION. THE COVARIANCE TABLES ARE PREVIOUSLY
C       COMPUTED FROM THE "TORSION BALANCE VERSION" OF COVAX
C       BY C.C. TSCHERNING AND TABULATED FOR READING INTO THIS
C       PROGRAM. THE FUNCTION HAS AS INPUT THE SPHERICAL DISTANCE
C       'D' AND THE COVARIANCE TYPE, 'ID'. IN THIS VERSION 'ID'
C       HAS THE FOLLOWING MEANINGS:
C
C         ID=1 : RADIAL/RADIAL GRADIENT AUTO-COVARIANCES
C         ID=2 : GRADIENT/HEIGHT ANOMALY CROSS-COVARIANCES
C         ID=3 : GRADIENT/GRAVITY ANOMALY CROSS-COVARIANCES
C
C       THE OUTPUT IS 'COVINT' WHICH RETURNS TO THE MAIN PROGRAM.
C
      IMPLICIT REAL *8(A-H,O-Z)
      COMMON /INTERP/COV(3,519)
```

```
      DO=0.DO
      DM=1.D-6
      IF (ID.EQ.0)GO TO 15
      DA=DABS(D)
      IF (DA.LT.DM)GO TO 18
      IF (ID.LT.0) GO TO 20
      MK=0
      GO TO 21
20    MK=1
      ID=ID*(-1)
21    OMIR=2.90882087D-4
      DR=D/OMIR
      X=DINT(DR)
      FRAC=DR-X
      IX=IDINT(DR)
C
C     IN THE NEXT STATEMENT, THE VALUE '519' CORRESPONDS TO THE
C     MAXIMUM SPHERICAL DISTANCE (IN THIS CASE, 8.5 DEGREES).
C
      IF (IX.GT.519) GO TO 17
      IX1=IX+1
      IX2=IX+2
      COVINT=COV(ID,IX1)+FRAC*(COV(ID,IX2)-COV(ID,IX1))
      IF (MK.EQ.1)COVINT=-COVINT
      GO TO 16
15    COVINT=0.DO
16    RETURN
18    COVINT=COV(ID,1)
      RETURN
17    WRITE(6,98)
98    FORMAT(///1X,'THE SPHERICAL DISTANCE IS TOO LARGE')
      STOP
      END
```

LIST OF REFERENCES

Applied Physics Laboratory, "GRM Spacecraft Description", APL report SDO-6721, Laurel, MD, 1983.

Colombo, O.L., "A World Vertical Network", Department of Geodetic Science & Surveying, Report No. 296, The Ohio State University, 1980

Colombo, O.L., "Numerical Methods for Harmonic Analysis on the Sphere", Department of Geodetic Science & Surveying, Report No. 310, The Ohio State University, 1981.

Colombo, O.L., "The Global Mapping of Gravity with Two Satellites", Geodetic Commission Netherlands, New Series, 7, No. 3, Delft, 1984.

Eren, K., "Spectral Analysis of Geos-3 Altimeter Data and Frequency Domain Collocation", Department of Geodetic Science and Surveying, Report No. 297, The Ohio State University, 1980.

Forward, R.L. et al, "Development of a Rotating Gravity Gradiometer for Earth Orbit Applications", Final Report, NASA Contract No. NAS 1-10945, NASA CR-11215, Washington, D.C., 1973.

Forward, R.L., "Review of Artificial Satellite Gravity Gradiometer Techniques for Geodesy", in "The Use of Artificial Satellites for Geodesy and Geodynamics", ed. by G. Veis, Athens, 1974.

Glaser, R.J., "Gravity Gradiometer Data Reduction", Thesis, California Institute of Technology, Pasadena, 1972.

Hajela, D.P., "A Simulation Study to Test the Prediction of 1°x1° Mean Gravity Anomalies Using Least Squares Collocation from the GRAVSAT Mission", Department of Geodetic Science and Surveying, Report No. 316, The Ohio State University, 1983

Hajela, D.P., "Accuracy Estimates of Gravity Potential Differences Between Western Europe and United State through LAGEOS Satellite Laser Ranging Network", Department of Geodetic Science & Surveying, Report No. 345, The Ohio State University, 1983.

Hein, G.W., "Numerical Investigations in Terrestrial Gravity Gradiometry", in "the Second International Symp. on Inertial Technology for Surveying and Geodesy", pp. 595-611, Calgary, 1981.

Hein, G.W. & Jochemczyk, H., "Reflections on Covariances and Collocation with Special Emphasis on Gravity Gradient Covariances", Man. Geod., V.4, pp. 45-86, 1979.

Heiskanen, W.A. & Moritz, H., "Physical Geodesy", Freeman & Co., San Francisco, 1967.

Ilk, K.H., "Ein Beitrag zur Dynamik ausgedehnter Körper - Gravitationswechselwirkung", Deutsche Geodätische Kommission, Series C, No. 288, Munich, 1983.

Jekeli, C. "An Investigation of Two Models for the Degree Variances of Gloal Covariance Functions", Department of Geodetic Science & Surveying, Report No. 275, The Ohio State University, 1978.

Jekeli, C., "On Optimal Estimation of Gravity from Gravity Gradients at Aircraft Altitudes", to appear in Reviews of Geophysics, 1985.

Jekeli, C. & Rapp, R.H., "Accuracy of the Determination of Mean Anomalies and Mean Geoid Undulations from a Satellite Gravity Field Mapping

Mission", Department of Geodetic Science & Surveying, Report No. 307, The Ohio State University, 1980.

Krarup, T. & Tscherning, C.C. "Evaluation of Isotropic Covariance Functions of Torsion Balance Observations", Bull. Geod., V. 57, pp. 180-192, 1984.

Krynski, J. & Schwarz, K.P., "Analysis of Satellite Gradiometry Data for Local Geoid Determination", Geodetic Institute at Graz, Report No. 26, pp. 1-25, Graz, Austria, 1977.

Melbourne, W.G. & Tapley, B.D., "The Geopotential Information in GPS Carrier-Phase Tracking from a Low Orbit Gravimetric Mission", EOS, V. 64, pp. 680 (abstract), 1983.

Metzger, E.H. & Jincitano, A., "Applications of Bell Rotating Accelerometer Gravity Gradiometers and Gravity Meters to Airborne or Land Vehicle Gravity Surveys" in "The Second International Symp. on Inertial Technology for Surveying and Geodesy", pp. 521-535, Calgary, 1981.

Moritz, H., "Advanced Physical Geodesy", Herbert Wichmann Verlag, Karlsruhe, 1980.

NASA, "The NASA Geodynamics Program: An Overview", NASA TP-2147, Washington, D.C., 1983.

NASA, "Announcement of Opportunity - Tethered Satellite System, A.O. No. OSSA-1-84, Washington, D.C., 1984.

National Academy of Science, "Applications of a Gravitational Satellite Mission", Washington, D.C., 1979.

Paik, H.J., "Superconducting Tensor Gravity Gradiometer for Satellite Geodesy and Inertial Navigation", J. Astr. Sci., V. 29, pp. 1-18, 1981.

Rapp, R.H., "Potential coefficient and Anomaly Degree Variance Modelling Revisited", Department of Geodetic Science & Surveying, Report No. 293, The State University, 1979.

Rapp, R.H., "The Earth's Gravity Field to Degree and Order 180 Using SEASAT Altimeter Data, Terrestrial Data, and Other Data", Department of Geodetic Science & Surveying, Report No. 322, The Ohio State University, 1981.

Rapp, R.H., "The Determination of Geoid Undulations and Gravity Anomalies from SEASAT Altimeter Data", JGR, V. 88, pp. 1552-1562, 1983.

Reed, G., "Application of Kinematical Geodesy for Determining the Short Wavelength Components of the Gravity Field by Satellite Gradiometery", Department of Geodetic Science & Surveying, Report No. 201, The Ohio State University, 1972.

Robbins, J.W., "Program to Compute all Components of the Gravity Gradient Tensor from Potential Coefficients", Department of Geodetic Science & Surveying Internal memo, The Ohio State University, 1984.

Rummel, R., "Downward Continuation of Gravity Information from Satellite-to-Satellite Tracking or Satellite Gradiometry in Local Areas", Department of Geodetic Science & Surveying, Report No. 221, The Ohio State University, 1975.

Rummel, R. & Colombo, O.L., "Gravity Field Determination from Satellite Gradiometry", submitted for publication in Bull. Geod., 1985.

Schwarz, K.P. & Lachapelle, G., "Local Characteristics of the Gravity Anomaly Covariance Function", Bull. Geod., V. 54, pp. 21-36, 1980.

Sünkel, H., "A Covariance Approximation Procedure", Department of Geodetic Science & Surveying, Report No. 286, The Ohio State University, 1979.

Tait, K.S., "Fast Collocation for Very Large Local Gravity Data Sets", The Analytical Sciences Corporation Report No. sp-9262, Reading, Mass., 1983.

Tscherning, C.C., "Covariance Expressions for the Second and Lower Order Derivatives of the Anomalous Potential, Department of Geodetic Science & Surveying, Report No. 225, The Ohio State University, 1976.

Tscherning, C.C., "Modifications of COVAX for the Direct Computation of Covariances of Torsion Balance Observations", Unpublished paper, 1983.

Tscherning, C.C. & Rapp, R.H., "Closed Covariance Expressions for Gravity Anomalies, Geoid Undulations, and Deflections of the Vertical Implied by Anomaly Degee Variance Models", Department of Geodetic Science & Surveying, Report No. 208, The Ohio State University, 1974.

Wells, W.C., "Spaceborne Gravity Gradiometers", NASA CP-2305, Washington, D.C., 1984.